




In silico study indicates antimalarials as direct inhibitors of SARS-CoV-2-RNA dependent RNA polymerase

Pawan Kumar Doharey^a, Vishal Singh^b, Mallikarjuna Rao Gedda^c, Amaresh Kumar Sahoo^b, Pritish Kumar Varadwaj^b  and Bechan Sharma^a

^aDepartment of Biochemistry, University of Allahabad, Allahabad, UP, India; ^bDepartment of Applied Sciences, Indian Institute of Information Technology Allahabad, Allahabad, UP, India; ^cDepartment of Biochemistry, Institute of Science, Banaras Hindu University, Varanasi, UP, India

Communicated by Ramaswamy H. Sarma

ABSTRACT

Coronavirus disease 2019 (COVID-19) caused by Severe Acute Respiratory Syndrome Coronavirus 2 (SARS-CoV-2) has caused a global pandemic. RNA-dependent RNA polymerase (RdRp) is the key component of the replication or transcription machinery of coronavirus. Therefore SARS-CoV-2-RdRp has been chosen as an important target for the development of antiviral drug(s). During the early pandemic of the COVID-19, chloroquine and hydroxychloroquine were suggested by the researchers for the prevention or treatment of SARS-CoV-2. In our study, the antimalarial compounds have been screened and docked against SARS-CoV-2-RdRp (PDB ID: 7BTF), and it was observed that the antimalarials chloroquine, hydroxychloroquine, and amodiaquine exhibit good affinity. Since the crystal structure of SARS-CoV-2-RdRp with its substrate is not available, poliovirus-RdRp crystal structure co-crystallized with its substrate ATP (PDB ID: 2ILY) was used as a reference structure. The superimposition of SARS-CoV-2-RdRp and poliovirus-RdRp structures showed that the active sites of both of the RdRps superimposed very well. The amino acid residues involved in the binding of ATP in the case of poliovirus-RdRp and residues involved in binding with the antimalarial compounds with SARS-CoV-2-RdRp were compared. In both cases, the conserved residues were found to be involved in establishing the interactions. The MMGBSA and molecular dynamic simulation studies were performed to strengthen our docking results. Further residues involved in binding of antimalarials with SARS-CoV-2-RdRp were compared with the residues involved in the SARS-CoV-2-RdRp complexed with remdesivir [PDB ID: 7BV2]. It was observed that co-crystallized remdesivir and docked antimalarials bind in the same pocket of SARS-CoV-2 -RdRp.

ARTICLE HISTORY

Received 24 July 2020
Accepted 1 January 2021

KEYWORDS

COVID-19; SARS-CoV-2-RNA dependent RNA polymerase; antimalarials; MD simulation; *in silico* inhibition

1. Introduction

Severe acute respiratory syndrome-related coronavirus-2 or SARS-CoV-2 causes disease COVID-19, which has been declared by WHO as a pandemic; the virus spreading as a global threat infecting millions of people with the death of 0.95 million people world over till 20th September 2020 have been reported by WHO (Coronavirus Disease (COVID-19) Situation Reports; Gorbalenya et al., 2020; Kupferschmidt & Cohen, 2020). The first epicenter of the COVID-19 was Wuhan, China, where the first case of COVID-19 was detected during December 2019. This disease has now spread in more than 200 countries in the world. Presently around 30.6 million cases of COVID-19 have been detected positive with around 6% morbidity and around 20% recovery (Coronavirus Disease (COVID-19) Situation Reports). Due to this outbreak of COVID-19, millions of peoples worldwide were forced to follow the quarantine and other safety measures and the COVID-19 has also severely affected the world economy (Gorbalenya et al., 2020; Kupferschmidt & Cohen, 2020). The

newly emerged COVID-19 caused by SARS-CoV-2 is more fatal and contagious than that due to the SARS-CoV-1 and Middle East Respiratory Syndrome Corona Virus (MERS-CoV) (B. Tang et al., 2020).

Coronavirus (CoV) belongs to a family of viruses containing positive-sense single-stranded RNA and causes respiratory infections in humans and some animals. All the CoVs are not very fatal and cause only mild respiratory disease. The SARS-CoV-1 and MERS-CoV emerged in 2002 and 2012 respectively, were very fatal causing the death of thousands of people (Centers for Disease Control and Prevention (CDC), 2003; van der Hoek, 2007). The SARS-CoV-1, MERS-CoV, and SARS-CoV-2 belong to the beta coronavirus class. These viruses attack the lower respiratory system and cause viral pneumonia. Besides this, they also affect the gastrointestinal system, liver, kidney, heart, and central nervous system finally leading to multiple organ failure (Su et al., 2016).

Presently, there is no effective and specific drug available for the treatment of COVID-19, except remdesivir and favipiravir which are successful up to some extent. Although many

antiviral drugs like remdesivir, favipiravir, ribavirin, penciclovir, galidesivir, lopinavir, rotinavir, etc. and many other drugs like hydroxychloroquine, chloroquine, dexamethasone, have been tested against COVID-19. Besides this many drugs and inhibitory compounds like tocilizumab, sarilumab, canakinumab, anakinra, baricitinib, ruxolitinib, heparin, fingolimod, etc. have been tested and also under trial which show immunomodulatory effects in COVID-19 patients.

Antiviral drugs remdesivir (Agostini et al., 2018; Brown et al., 2019; Sheahan et al., 2020; Wang et al., 2020), favipiravir (Agostini et al., 2018; Wang et al., 2020), ribavirin (Al-Tawfiq et al., 2014; Falzarano et al., 2013; Wang et al., 2020), penciclovir (Wang et al., 2020), galidesivir (Agostini et al., 2018; Wang et al., 2020) are known inhibitors of RdRps, while lopinavir (de Wilde et al., 2014; Kim et al., 2016; Sheahan et al., 2020) and rotinavir (Kim et al., 2016; Sheahan et al., 2020) are known inhibitors of main protease protein (M^{Pro}) of coronavirus. The other drugs like tocilizumab, sarilumab, canakinumab, anakinra, etc. are monoclonal antibodies and immunomodulatory in nature, these antibodies are under trial for the treatment of COVID-19 (Arabi et al., 2020; Lamb & Deeks, 2018; Ozdogan & Ugurlu, 2017; Ridker et al., 2017). Tocilizumab and sarilumab are IL-6 receptor inhibitors while canakinumab and anakinra target IL-1 and fight with cytokine storm.

The coronavirus belongs to the coronaviridae family, which includes viruses containing RNA as their genetic material. The genome of coronaviruses is the largest among different groups of other viruses, The SARS-CoV-2 has around ~30kb long genome that encodes for many nonstructural (NSPs) and structural proteins (F. Wu et al., 2020). In the case of SARS-CoV-2, 16 NSPs are expressed from the ORF1a and ORF1ab gene. This gene is located at the 5' end of the virus genome (Wu et al., 2020). Different NSPs have different functions and play roles in the survival and progression of the coronavirus.

The level of mortality caused by the present COVID-19 has been reported to be around 1-6%. It is much less than that caused by SARS and MERS with a mortality rate of 10 and 40%, respectively. However, SARS-CoV-2 has a very high replication number as compared to SARS-CoV-1 and MERS-CoV, which is responsible for the rapid spread of the disease globally (Liu et al., 2020). Due to a lack of specific drugs for COVID-19 therapy, the patients are being given only symptomatic treatment or with some already known antivirals. It has resulted in a low recovery rate of the patients. Therefore, there is an urgent need to discover some novel compounds for the treatment and control of COVID-19.

The nsp12 of SARS-CoV-2 recognized as RNA dependent RNA polymerase (RdRp) is an important protein for RNA replication and transcription. It plays a key role in virus replication in the infected cells. The nsp12 (RdRp) has minimal activity but nsp7 and nsp8 are required for its optimal function. The nsp7 and nsp8 act as their co-factor and thus help greatly to accelerate its polymerase function of nsp12 (Ahn et al., 2012).

In the present scenario of our quest to search for a novel anti-COVID-19 agent, the repurposing of drugs could be the

best way towards disease management. Most of the known antiviral drugs against viral RdRps have proved to be ineffective as many of them are nucleoside analogues. Since nsp14 of SARS-CoV-2 consists of an exonuclease domain with proofreading activity, it removes any wrong nucleotide (nucleoside/nucleotide analogue) addition (mis-insertion or mis-incorporation) into the growing nascent RNA chain during replication or transcription (Bouvet et al., 2012; Ma et al., 2015; Minskaia et al., 2006; Snijder et al., 2003).

Since remdesivir and favipiravir is a nucleoside analogue and nsp14 of SARS-CoV-2 has proofreading activity, the mis-insertion or mis-incorporation of it in the growing nascent RNA chain and hence its termination may not be possible, which might lead to failure of action of this drug. So, the application of any non-nucleoside analogue(s) as a drug may be a better approach to arrest SARS-CoV-2 progression.

Chloroquine and hydroxychloroquine are the antimalarial compounds, as they efficiently terminate the life cycle of the malarial parasites. These drugs are also used to treat amoebiasis that is occurring outside the intestines, rheumatoid arthritis, and lupus erythematosus. As an antimalarial agent, these molecules accumulate in the parasite's food vacuole, terminate the process of formation of hemozoin due to polymerization of heme, and form a heme-chloroquine complex. This complex is extremely toxic to the schizonts and induces lysis of parasites' membranes and kills the parasite (Chong & Sullivan, 2003). Besides, these antimalarials have also been reported to be anti-inflammatory and antiviral in nature. As anti-rheumatoid agents, these drugs cause interruptions in the process of 'antigen processing' in macrophages and other antigen-presenting cells. This event results in decrease in the formation of peptide-MHC protein complexes as well as downregulation of the immune response against autoantigenic peptides (Fox, 1993). Amodiaquine is a drug used to treat malaria caused by *Plasmodium falciparum*. The side effects of amodiaquine are similar to those of chloroquine and hydroxychloroquine. These drugs are included in the World Health Organization's List of Essential Medicines, the safest and most effective medicines needed in a health system.

In this study, we have proposed that three well-known antimalarial compounds viz.; chloroquine, hydroxychloroquine, and amodiaquine may be used as the direct inhibitor of the SARS-CoV-2-RdRp. In order to test our hypothesis, we have analyzed the extent of binding of these molecules with the SARS-CoV-2-RdRp using *in silico* approach.

2. Materials and methods

2.1. Modelling platform

All the computational work was performed using the Schrodinger suite Maestro v12.0, Schrodinger, LLC, New York, NY, 2019-2 version, package including LigPrep, Protein preparation wizard, GlideXP docking, grid generation, free energy calculations, absorption, distribution, metabolism, excretion, toxicity (ADMET), and MD simulations. A high-performance cluster computer with Centos Linux operating system was used for this study.

2.2. Ligand preparation

Libraries of coronavirus specific compounds, antimalarials and FDA approved (2016–2019) drugs were downloaded or manually prepared, all the downloaded compounds were saved in mol or sdf format and further converted into pdb format. Energy minimization was done using the OPLS-2005 force field (LigPrep, Glide-v8.3 Schrodinger, LLC, New York, NY, 2019-2). Further ligands were processed using LigPrep 4.4 module a part of the Schrodinger suite which can generate different types of structures from each input structure with various tautomers, ionization states, ring conformations, and stereochemical characteristics (Shan et al., 2005). Three, isomers were prepared for each compound with the lowest energy conformation.

2.3. Protein and grid preparation

The crystal structure of SARS-CoV-2-RNA dependent RNA polymerase (PDB ID: 7BTF) was retrieved from RCSB protein data bank (<https://www.rcsb.org>). Protein preparation for the docking and other *in silico* studies was carried out using the protein preparation wizard of Maestro program v10.2, a part of the Schrodinger suite (Schrodinger, LLC, New York, NY, 2019-2). Default parameters were used to prepare the protein/receptor (Sastry et al., 2013). The active site of the protein was identified using the program site map and center of the grid kept around the conserved residues (Asp623, Thr680, Asn691, Val557) of RdRps. Grid box was created using program Glide v8.3, Schrodinger, LLC, New York, NY, 2019-2 (Halgren et al., 2004). Dimensions of the inner box were kept $X=20$, $Y=20$, $Z=20$, and dimensions of the outer box were as kept $X=30$, $Y=30$, $Z=30$, and center $XYZ=137.49/151.91/150.91$.

2.4. Molecular docking and screening

Flexible docking was performed to evaluate the docking score, Glide score, and Glide e-model of all the prepared ligands against the predicted binding site of SARS-CoV-2-RdRp (PDB ID: 7BTF) using Glide v8.3, Schrodinger, LLC, New York, NY, 2019-2. Glide generates multiple poses for every ligand which are initially filtered by the spatial fit on the protein grid or active site and are checked for the complementarity of interaction using the ChemScore function.

The poses that pass the initial filter were minimized with respect to the receptor grid using OPLS-AA nonbonded ligand–receptor interaction energy. Once the energy is calculated Glide score multiligand scoring function assigned scores to the poses. GLIDE docking was carried out in standard-precision (SP) mode, and the molecules that bind to the receptors with good docking scores and negative binding energy were used for further analysis.

Docking results were assessed based on the scoring function given by Glide score or Glide G-score, which can be

represented as:

$$\begin{aligned} \text{GScore} = & 0.065 \times \text{Vander Waals energy} + 0.130 \\ & \times \text{Coulomb energy} + \text{Lipo} + \text{H bond} \\ & + \text{Metal} + \text{BuryP} + \text{RotB} + \text{Site} \end{aligned}$$

where Lipo=hydrophobic interactions, Metal=metal binding, BuryP=buried polar group penalty, RotB=penalty for freezing rotatable bonds, and Site=polar interactions existing in the active site represented.

Analysis of amodiaquine, hydroxychloroquine, and chloroquine in comparison to ATP substrate, was carried out based on docking scores and involved interacting residues of the active site.

2.5. Absorption, distribution, metabolism, excretion, and toxicity

Evaluation of ADMET (Absorption, Distribution, Metabolism, Excretion, and Toxicity) properties is an essential parameter for the development of a pharmacologically active compound. ADMET is required for the determination of the safety and efficacy parameter of a new drug. ADMET properties were determined by using the Qikpro v4.4 module (Schrodinger, LLC, New York, 2019).

2.6. Molecular mechanics-generalized born surface area

Compounds showing best docking score and suitable ADMET properties were selected for Prime molecular mechanics-generalized born surface area (MMGBSA) for their ligand binding energy calculation (Prime, version 2.1, Schrödinger, LLC, New York, 2011) (Hayes & Archontis 2012). The Receptor-ligand complex structures obtained from molecular docking were used for this process. The obtained ligand poses were minimized using the local optimization feature in Prime, whereas the energies of the complex were calculated with the OPLS-2005 force field and Generalized-Born/Surface Area continuum solvent model. During the simulation process, the ligand strain energy was also considered.

2.7. Molecular dynamics simulations study

Desmond a module of Schrodinger suite (Maestro-Desmond Interoperability Tools, version 4.1, Schrödinger, New York, 2019-1) was used to study the conformational stability of receptor-ligand complex (Bowers et al., 2006). MD simulations of amodiaquine, hydroxychloroquine, chloroquine, and ATP in complex with SARS-CoV-2-RDRP (PDB ID: 7BTF) were performed. Each simulation was performed for 100 ns. Protein–ligand root-mean-square deviation (RMSD), protein–ligand contact bar graph, root mean square fluctuation (RMSF), simulation quality analysis (SQA), and simulation event analysis (SEA) were analyzed to assess the stability and conformational behavior of the protein–ligand complex throughout the 100 ns simulation.

2.8. System building

Before MD simulation, processing of protein–ligand complexes and refinement of side-chain amino acid residues were performed using Maestro (Schrödinger, LLC, New York, NY, 2019-2). All the missing atoms were also added and after the processing, the complex was introduced to Desmond. The TIP3P water model was added to the complex system using the solvation tab (Jorgensen et al., 1983). An orthorhombic box of $10 \times 10 \times 10 \text{ \AA}$ dimension was built to cover the entire complex with OPLS_2005 force-field (optimized potential for liquid simulations) and SPC (simple point charge) solvent system. Na^+/Cl^- ions were added to balance and neutralize the system and to mimic and stabilize the real-time and in vitro environment, 0.15 M NaCl was additionally provided during the simulation (Bowers et al., 2006). Before proceeding for the final molecular dynamics simulation run, the systems were minimized by employing applying 1 kcal/mol Å of convergence threshold with 2000 iterations along with pre-equilibration by using ingrained relaxation module built-in Desmond. Furthermore, the complexes were subjected to 300 K and 1 Bar pressure for 100 ns NPT ensemble with a recording interval of 10 ps.

2.9. Molecular dynamics

Molecular dynamics simulations of the complexes were performed after the system-building of the 7BTF–ligand complex was completed. The build system of the best-screened complex was loaded for MD simulation for 100 ns. All the parameters like recording interval (ps), energy, trajectory, NPT (temperature – 300 K, pressure = 1.01325 bar) were followed as the default value, and the checkpoint interval of the simulation was kept 240.06 ps. MD simulation was performed using Desmond, Schrodinger, LLC, New York, NY, 2019-1 (Bowers et al., 2006).

3. Results

3.1. SARS-CoV-2-RdRp structure

Recently, Gao and coworkers solved the structure of RdRp of SARS-CoV-2 using the Cryo-EM technique (Gao et al., 2020). Since sequences of SARS-CoV-1 and SARS-CoV-2 viruses are very much similar, the structures of their RdRps were also found very much similar. The core structure of RdRps of SARS-CoV-2, SARS-CoV-1, and many other viruses like hepatitis C virus, poliovirus (PV), dengue virus, etc. displays large similarity and conservation (Ago et al., 1999; Hansen et al., 1997; Yap et al., 2007).

The nsp12 of SARS-CoV-2 contains two major domains one is RdRp and another is nidovirus-unique N-terminal extension domain. Nidovirus-unique N-terminal extension domain (residues D60-R249) possesses nidovirus RdRp-associated nucleotidyltransferase. The RdRp domain (S367-F920) is a right-hand shaped domain that contains palm, finger, and thumb subdomains (Lehmann et al., 2015), and these two domains are connected by an interface domain (A250-R365) (Gao et al., 2020).

The nsp7 and nsp8 are associated proteins with the nsp12 and these are important for the function of the nsp12 or RdRp. Nsp7 and nsp8 of SARS-CoV-2 have the conserved structure as in SARS-CoV-1 (Kirchdoerfer & Ward, 2019; Zhai et al., 2005). The crystal structure that we used in our study is a complex of nsp12, nsp8, and nsp7 (PDB ID: 7BTF), which exhibits large similarity with the complex contained by SARS-CoV-1 (PDB ID: 6NUR) with an RMSD value of 0.82 (Gao et al., 2020). Although nsp7 and nsp8 increases the activity of RdRp but the main active site essential for replication is located in the nsp12/RdRp. Since our focus was on finding out the specific inhibitor against SARS-CoV-2-RdRp that is why during the preparation of protein for our *in silico* studies, we removed the nsp7 and nsp8 parts from this structure (PDB ID: 7BTF) and worked only with nsp12.

The polymerase domain of the different viral polymerase families has a very conserved structure and this is formed by three different subdomains finger, palm, and thumb (Figure 1(a)) (McDonald, 2013). In the case of SARS-CoV-2, the finger subdomain comprises the residues L366-A581 and K621-G697, the palm subdomain comprises the residues T582-P620 and T680-Q815 and the thumb subdomain comprises the residues H816-E920 (Gao et al., 2020). The presence of metal ions is also observed in most of the viral polymerases which synthesize RNA (Appleby et al., 2015; P. Gong & Peersen, 2010).

The RdRp from the polymerase family of viruses has a conserved active site which is made up of seven conserved polymerase motifs A to G. In SARS-CoV-2-RdRp, motif A comprises the residues 611–626 and has a divalent cation binding residue Asp618, which is a conserved residue in most of the RdRps like Hepatitis C virus nonstructural protein 5B (NS5B) (residue Asp220) and PV-RNA-dependent RNA polymerase (3D^{pol}) (residue Asp233) (Appleby et al., 2015; Gong & Peersen, 2010). Another conserved catalytic residues in most of the RdRps remains present in motif C, in the case of HCV ns5b residues 317-GDD-319 and in the case of PV 3Dpol residue 327-GDD-329 (Appleby et al., 2015; Gong & Peersen, 2010). In the case of SARS-CoV-2-RdRp Motif C residues, 753-FSMMLSDDAVVCFN-767 possesses the catalytic residues 759-SDD-761 in the turn between two β -sheets (Gao et al., 2020). The first residue in this can be serine or glycine depending on the positive and negative RNA sense strands; i.e. glycine in the case of the positive-sense RNA strand and serine in the case of the negative-sense RNA strand.

As previously reported in the polymerase domain of RdRps of different polymerase virus (SARS-CoV-1 and for other RNA polymerases such as HCV and PV polymerase) the arrangement of the template or primer entry path, the nucleoside triphosphate entry channel, and the newly synthesized strand exit path is positively charged, solvent accessible and opens in a central cavity. At this central cavity, the motifs of RdRps perform the template-directed RNA synthesis (Gong & Peersen, 2010). A similar configuration of all the channels/tunnels and their environment were observed in the RdRp of SARS-CoV-2 that we selected for our study (Gao et al., 2020). The primer and the template reach the

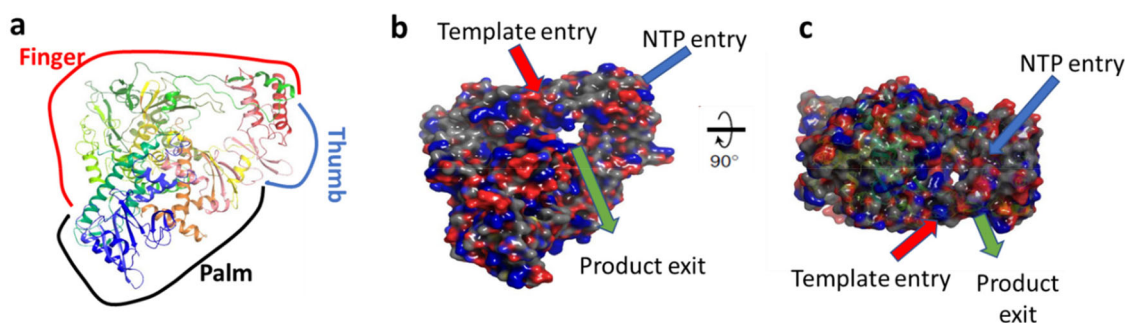


Figure 1. General structural representation of SARS-CoV-2-RdRp (PDB ID: 7BTF). (a) Multicolor ribbon representation showing thumb, finger, and palm domains. (b) Solid surface representation in the same pose showing template entry, NTP entry, and product exit sites. (c) Solid surface representation at 90° angle showing template entry, NTP entry, and product exit sites.

active site through different channels and the nascent RNA exit through a separate tunnel (Figure 1(b,c)).

The NTP entry channel residues are hydrophilic in nature and they are part of motif F, the main residues are K545, R553, and R555. The RNA template entry channel is different and it is composed of motif F and G, and it reaches to active site composed of motifs A and C. Primer strand is supported by motif E and thumb domain during the process of RNA synthesis and the template and product hybrid exit through the exit tunnel, exit tunnel is situated at the front side of the RdRp (Gao et al., 2020).

3.2. Comparison of substrate binding mode in SARS-CoV-2-RdRp and PV-RdRp

The nucleotides act as the substrates for the RdRps. It is previously known that ATP is the natural substrate for SARS-CoV-1-RdRp (te Velthuis et al., 2010). In the case of SARS-CoV-2-RdRp, ATP and other nucleotides also serve as the substrate. However, the crystal structures of ATP bound SARS-CoV-1-RdRp and SARS-CoV-2-RdRp are not available, so we used PV ATP-bound RdRp (PDB ID: 2ILY) as a reference structure for the ATP binding site and ATP binding residues because the active sites of most of the RdRps are very conserved (Figure 2(a,b)) (Ferrer-Orta et al., 2006; Mönttinen et al., 2014; Ng et al., 2008; te Velthuis, 2014).

In PV-RdRp (PDB ID: 2ILY) the adenosine part of the ATP interacts or is surrounded by the residues like Lys61, Lys159, Leu175, Arg174, Isoleu176, Glu177, Asp238, and Ser288. The triphosphate part of the ATP interacts or is surrounded by most of the positively charged residues like Lys167, Arg163, Lys359, Arg174, Lys172, Thr235, Gly236, Tyr237, Asp233, Asp297, Asp328. Mg^{+2} was found to interact with Asp328 negatively charged residue.

To guesstimate the binding of ATP with the SARS-CoV-2-RdRp, we superimposed the RdRp of PV co-crystallized with ATP (PDB ID: 2ILY) and SARS-CoV-2-RdRp (PDB ID: 7BTF, without nsp7 and nsp8) without any substrate or inhibitor (Figure 2(c)). It was observed that both the structures superimposed very well at the active site region, since the size of both RdRps is quite different, PV-RdRp has 461 amino acid while the SARS-CoV-2-RdRp has 932 amino acids, that is why they did not fully overlap but the active site of both the RdRps are very well superimposed (Figure 2(a)). Over this

superimposed structure, we analyzed the probable residue involved in ATP interaction with the SARS-CoV-2-RdRp.

On the superimposition of the two structures, it was observed that the nucleoside part of the ATP was found surrounded by the residues Asp623, Ser682, Val557, Thr556, Arg555, Arg553, Arg555, Ala547, Lys545, and Ala558. and the triphosphate part of the ATP found surrounded by residues Asp618, Asp760, Lys621, Asn691, Lys551, Tyr619, Ser549, Arg555, Cys622, and Arg553 (Figure 3(b)).

Superimposition of the two structures again indicated the conservation of the active site of the two RdRps, and also gives a view to the probable binding of the ATP in the SARS-CoV-2-RdRp. This also shows the most of the residues present around the triphosphate part of the ATP are hydrophobic and most of the residues present around the nucleoside part of the ATP are positively charged.

3.3. SARS-CoV-2-RdRp grid preparation and structure-based virtual screening

After the determination of important residues that seem important with the interaction of ATP with the RdRp. A grid was prepared in the SARS-CoV-2-RdRp protein around this active site area. A self-prepared library of antimalarials, antivirals, and nucleotides of 300 compounds was screened against SARS-CoV-2-RdRp. Surprisingly, we found that antimalarial compounds chloroquine, hydroxychloroquine, and amodiaquine were showing good binding affinity with the SARS-CoV-2-RdRp as shown in Table 1.

3.4. Comparison of binding sites for SARS-CoV-2-RdRp substrate ATP and antimalarials

After docking and screening the binding of amodiaquine, hydroxychloroquine, and chloroquine were compared with the binding of the ATP within SARS-CoV-2-RdRp. It was observed that all three compounds bind in the same cavity where ATP binds in SARS-CoV-2-RdRp predicted binding site. On deep analysis, it was observed that all three compounds shared mostly the same residues involved in the interaction as in the case of ATP with SARS-CoV-2-RdRp (Figure 4).

ATP interacts strongly (makes H-bond) with the Thr680, Asp623, Asp760, Ser759, Ala550, Arg553, Arg555, while the surrounding residues are Ser682, Asn691, Val557, and

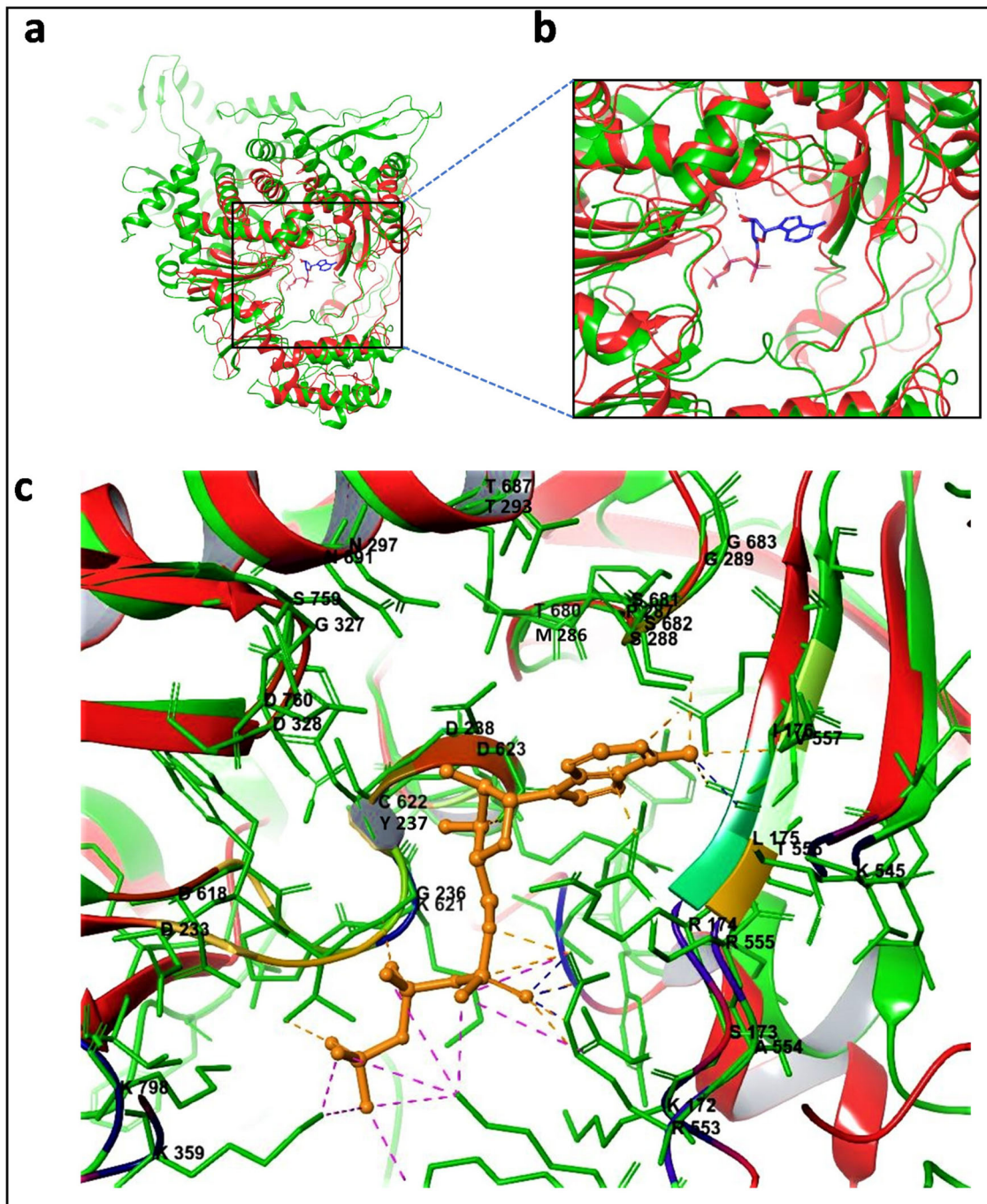


Figure 2. Active site superimposition of SARS-CoV-2-RdRp (932 residues) and poliovirus-RdRp (461 residues). (a) Full-length protein superimposition, green represents SARS-CoV-2-RdRp and red represents poliovirus-RdRp with ATP. (b) Enlarged view of the superimposed active site area. (c) Superimposed residues of SARS-CoV-2-RdRp and poliovirus-RdRp, poliovirus-RdRp has ATP with it, and SARS-CoV-2-RdRp is without any substrate or inhibitor.

Cys622. On comparison of ATP binding with SARS-CoV-2-RdRp with the ATP binding with the PV-RdRp, it was observed that all/most of the residues are perfectly superimposed on the residues which are making contacts with PV-RdRp. This shows the binding and docking of ATP with COVID-19-RdRp in our case is quite accurate (Figure 4(a)).

In the case of amodiaquine, it strongly interacts with the residues Asp623, Thr680, and Asp760, and surrounded by residues Arg553, Arg555, Thr556, Ser 681, and Asn691. This shows that amodiaquine also binds in the same pocket where ATP binds and the residues involved in the interaction and surrounding residues are almost common (Figure 4(b)).

In the case of hydroxychloroquine, it strongly interacts with the residues Asp623 and Thr680 while it is surrounded by Val557, Lys621, Cys622, Asp760, Ser 682, Asn691, Arg553, Arg555, and Thr556. This also shows that hydroxychloroquine also binds in the same pocket in which ATP and amodiaquine bind and most of the residues interacting with hydroxychloroquine are common as in ATP and amodiaquine (Figure 4(c)). Chloroquine also binds in the same pocket and shows strong interactions with the Thr680, Asp 623, and Asn691, and the surrounding residues are also the same as in the case of amodiaquine and hydroxychloroquine (Figure 4(d)).

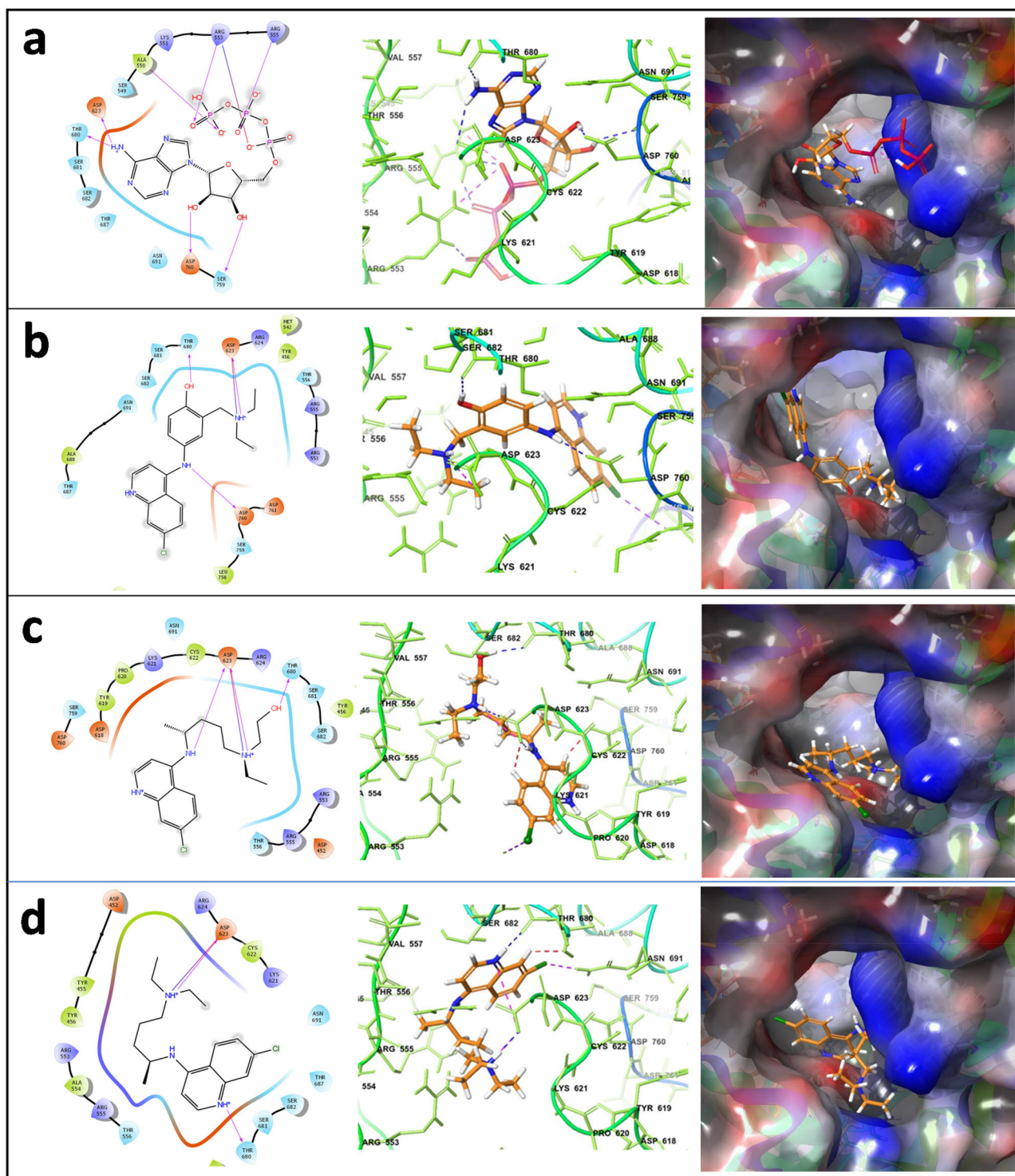


Figure 4. The 2D, 3D, and surface interaction diagram of ATP and antimalarial molecules with the SARS-CoV-2-RdRp protein-based Doc. Panel (a) with ATP, (b) with amodiaquine, (c) with hydroxychloroquine, and (d) with chloroquine are shown here. 2D diagrams were prepared using GLIDE and only H-bond interactions are represented here. In the 3D diagrams, SARS-CoV-2-RdRp is illustrated with thin tubes for clarity, residues that directly contact with ATP and other antimalarials (within 5 Å of the molecule) are illustrated in thin stick models.

Table 2 The MM/GBSA binding energy scores and individual energies contributing in MMGBSA, for ATP and antimalarials.

Compound ID/Compound	MMGBSA dG Bind	MMGBSA dG_{Bind} Contributions				
		Coulomb	Covalent	H-bond	Solv GB	vdw
ATP	-26.3923	-19.1303	2.9973	-11.4068	38.1262	-33.1463
Amodiaquine	-39.0692	96.5982	10.3077	-3.0686	-83.1767	-32.7672
Hydroxychloroquine	-46.8734	86.5922	2.7790	-1.1339	-81.9524	-29.5633
Chloroquine	-42.6538	116.8878	9.1116	-1.6630	-111.0809	-27.8017

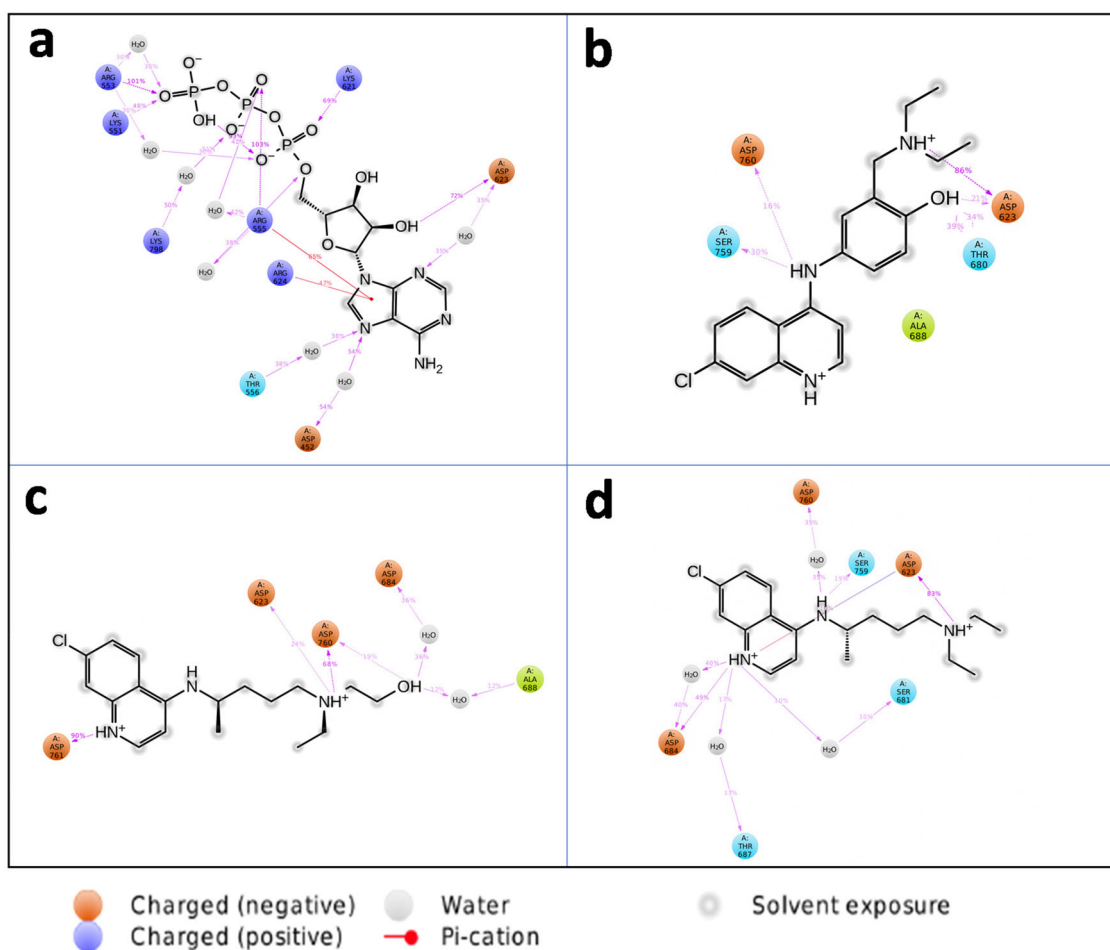


Figure 5. Post-MD simulations detailed ligand atom interactions with the SARS-CoV-2-RdRp with ATP and antimalarials. Interactions that occur more than 30.0% of the simulation time in the selected trajectory (0.00 through 100 ns) are shown. SARS-CoV-2-RdRp showing interaction (a) with ATP, (b) with amodiaquine, (c) with hydroxychloroquine, and (d) with chloroquine. Orange circle: charged (negative), Blue circle: charged (positive), White circle: water, and Red circle with bar represents Pi-cation.

play important roles in the interaction of ATP with RdRp. All of these residues make the H-bond with the ATP (Figure 5(a)). The residues, Arg624 and Arg555, make the pi-pi interaction with the adenosine part of the ATP. Asp623 makes the H-bond with the ribose part of the ATP. The ribose part of the ATP donates an H-bond to the Asp623. Lys621, Arg553, Arg555, Lys551, and Lys798 all make H-bond with the triphosphate part of the ATP, they all donate H-bond to the triphosphate part of the ATP. Asp623 and Lys621 belong to motif A and Arg553, Arg555, and Lys551 residue belong to motif F.

Protein-ligand contacts (SARS-CoV-2-RdRp-ATP) (Figure 6(a)) indicate that Asp452, Lys551, Arg553, Arg555, Thr556, Lys621, Asp623, Arg624, and Lys798 exhibit strong interaction with the ATP throughout the simulation. It was observed that Lys551, Arg553, Arg555, Thr556, Lys621, and Asp623, show strong H-bond interaction, while Asp452, Lys551, Arg553, Arg555, Thr556, Lys621, and Asp623 show water bridges as well as H-bond. Arg624 and Arg555 also indicate strong hydrophobic interactions. Lys798 mainly shows water bridges and hydrophobic interaction but no direct H-bond interaction.

On analysis of total contacts (SARS-CoV-2-RdRp-ATP) during the full simulation time, it was observed that the

maximum number of bonds or contacts formed from 0 to 13 ns and the maximum number of contacts were observed at 6–12 ns after that total number of contacts seems to decrease till 23 ns after that it increases again and remains stable till the end of 100 ns of simulation (Supporting information Figure 1(a)). The timeline representation of the interactions and contacts shows that Asp452, Lys551, Arg553, Arg555, Lys621, Asp623, and Arg624 make the H-bond interaction with the ATP throughout the 100 ns simulation. However, in the starting up to about 16 ns Asp452, Lys621, and Asp623 show fewer H-bond interactions, after that interactions become stronger till the end of the simulation. Residues Lys551, Arg553, Arg555, and Thr556 show good H-bond interaction throughout the MD simulation. Arg624 and Arg555 also make the pi-pi interaction with the adenosine part of the ATP (Supporting information Figure 1(b)).

RMSD analysis of the SARS-CoV-2-RdRp-ATP complex showed that the fluctuations in the protein-RMSD became stable around 15 ns and the fluctuations in the ligand-RMSD became stable after 22 ns and both remained stable till the end of 100 ns simulation. The RMSD mean for backbone, side-chain, and ligand were calculated to be 2.827 ± 0.216 , 3.696 ± 0.231 , and 2.123 ± 0.195 Å, respectively (Figure 7(a)).

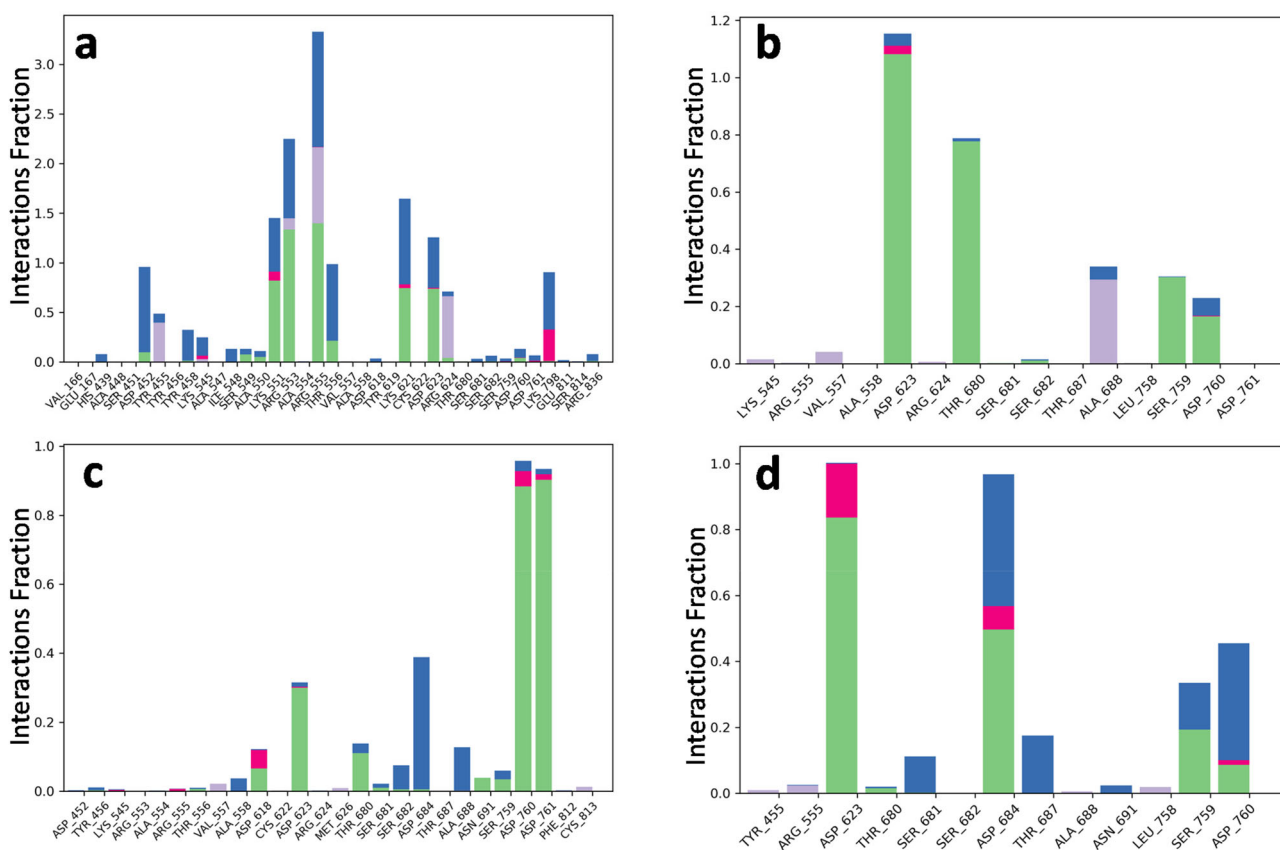


Figure 6. Protein–ligands contacts histogram showing important interacting residues of SARS-CoV-2-RdRp with ATP and antimalarials during and after 100 ns MD simulation. X-axis showing residues and Y-axis showing interactions fraction. (a) Interactions with ATP, (b) interactions with amodiaquine, (c) interactions with hydroxychloroquine, and (d) interactions with chloroquine. Different colors in the histogram representing different types of bond interactions fraction. The green color representing H-bond, violet representing hydrophobic, pink representing ionic, and blue representing water bridges, interactions fraction.

3.8.2. SARS-CoV-2-RdRp/amodiaquine

Post MD simulation interaction diagram shows the residues Asp623, Thr680, Asp760, and Ser759 play important role in the interaction of amodiaquine with SARS-CoV-2-RdRp, these all residues make the H-bond with the amodiaquine (Figure 5(b)).

Protein–ligand contacts (SARS-CoV-2-RdRp-amodiaquine) (Figure 6(b)) demonstrate that Asp623, Thr680, Ser682, Ala688, and Asp760, make strong interactions during the simulation. It was observed that Asp623, Thr680, Ser759, and Asp760 exhibit strong H-bond interaction, while Ala688 and Asp760 show strong hydrophobic interactions. Asp623, Thr680, Ala688, and Asp760 also participate in making partial water bridges. Ala688 also shows strong hydrophobic interaction.

Upon analysis of the total contacts (SARS-CoV-2-RdRp-amodiaquine) over the full simulation time, it was observed that a similar number of bonds or contacts were found throughout the 100 ns of simulation (Supporting information Figure 2(a)). The timeline representation of the interactions and contacts demonstrate that Asp623, Thr680, Ala688, and Asp760 make the H-bond interaction throughout the 100 ns of simulation. While Ser759 shows interactions up to 75 ns simulation after that these interactions become weak (Supporting information. Figure 2(b)).

RMSD analysis of the SARS-CoV-2-RdRp-Amodiaquine complex demonstrated that the fluctuations in the protein-

RMSD became stable around 25 ns and after that remained stable till the end of 100 ns simulation, and the fluctuations in the ligand-RMSD also became stable after 25 ns and remained stable up to 72 ns. After a fluctuation, this became again stable from 80 ns and remained stable till the end of the simulation. The RMSD mean for backbone, side-chain, and ligand were calculated and found to be 2.947 ± 0.276 , 3.807 ± 0.306 , and 0.935 ± 0.271 Å, respectively (Figure 7(b)). The SEA, SQA, and protein–ligand interaction during the simulation also supported the same finding.

3.8.3. SARS-CoV-2-RdRp/hydroxychloroquine

Post MD simulation interaction diagram displays the residues Asp623, Asp684, Asp760, and Asp761 play an important role in establishing the interaction of hydroxychloroquine with SARS-CoV-2-RdRp. These all residues of SARS-CoV-2-RdRp make the H-bond with the hydroxychloroquine (Figure 5(c)). Asp761 received an H-bond from the chloroquinoline part of the hydroxychloroquine, while ASP623, Ala688, and Asp760 interacted through the H-bonds with the remaining part of the hydroxychloroquine both receive H-bond. Asp623 belongs to motif A, Asp760 and Asp761 belong to motif C of SARS-CoV-2-RdRp.

Protein–ligand contacts (SARS-CoV-2-RdRp-hydroxychloroquine) (Figure 6(c)) indicate that Ala558, Asp618, Asp623,

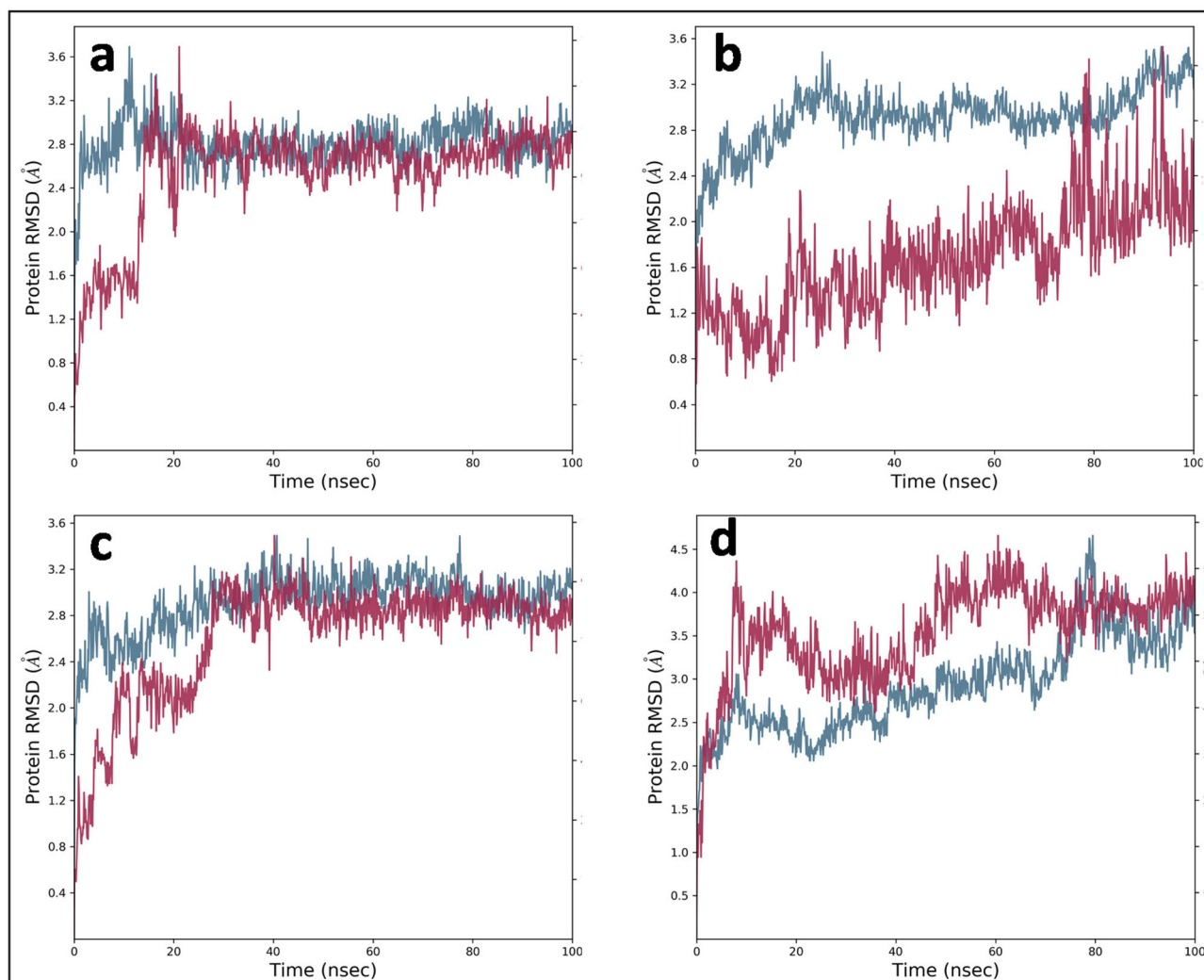


Figure 7. RMSD of protein and protein–ligand complexes. Here, the blue graph represents protein RMSD and the maroon graph represents protein–ligand complex RMSD. (a) SARS-CoV-2-RdRp alone and with ATP in a complex, (b) SARS-CoV-2-RdRp alone and with amodiaquine in a complex, (c) SARS-CoV-2-RdRp alone and with hydroxychloroquine in complex, and (d) SARS-CoV-2-RdRp alone and with chloroquine in complex.

Thr680, Ser681, Ser682, Asp684, Ala688, Asn691, Ser759, Asp760, and Asp761 make strong interactions during the simulation. It was observed that Asp618, Asp623, Thr680, Ser681, Asn691, Ser759, Asp760, and Asp761 make H-bond interactions. In these residues, Asp618, Asp623, Thr680, Asp760, and Asp761 exhibit strong interaction. Asp623, Thr680, Ser681, Ser759, Asp760, and Asp761 establish water bridge interactions along with H-bond interactions. Asp558, Ser682, Asp684, and Ala688 show only water bridges. Asp618, Asp760, and Asp761 also exhibit ionic interactions along with H-bond interactions.

On analysis of total contacts (SARS-CoV-2-RdRp-hydroxychloroquine) over the full simulation time, it was observed that the maximum number of bonds or contacts formed from 0 to 30 ns and maximum between 0 and 10 ns, after that at 20, 30, and 50 ns high interactions were observed. After 50 ns interactions become constant and remain until the end of the 100 ns simulation (Supporting information Figure 3(a)). The timeline representation of the interactions and contacts represent that Asp623 makes the H-bond interaction up to 27 ns of simulation. Asp618 also shows interaction up to 10 ns strongly after that this shows interaction

via H-bond at different times. Thr680, Ser681, and Ser682 also exhibit good H-bond interaction up to 25 ns. Asp760 shows H-bond interaction throughout the simulation but after 27 ns this shows strong interaction. Asp761 shows very strong H-bond interaction from 8 ns to the end of the simulation (Supporting information Figure 3(b)).

RMSD analysis of the SARS-CoV-2-RdRp-hydroxychloroquine complex showed that the fluctuations in the protein-RMSD became stable around 4 ns and of the ligand-RMSD became stable after 17 ns and both remained very stable till the end of 100 ns simulation. However, ligand-RMSD showed a fluctuation between 20 and 30 ns and after that, it became stable again. The RMSD mean for backbone, side-chain, and ligand were predicted to be 2.947 ± 0.261 , 3.770 ± 0.297 , and 2.006 ± 0.278 Å, respectively (Figure 7(c)).

3.8.4. SARS-CoV-2-RdRp/chloroquine

Post MD simulation interaction diagram shows the residues Asp623, Asp684, Thr687, Ser681, Ser759, and Asp760 playing important role in the interaction of chloroquine with SARS-CoV-2-RdRp, these all residues make the H-bond with the

Table 3. Active site residues comparison table.

SARS CoV2 -RDRP (PDB ID:7BTF)	Poliovirus -RDRP (PDB ID:2ILY)
Ser759	Gly327
Asp618	Asp233
Ser549	Arg163
Ala547	Glu161
Ala554	Ser173
Gly683	Gly289
Thr687	Thr293
Asn691	Asn297
Cys622	Tyr237
Lys621	Gly236
Lys545	Lys159
Arg555	Arg174
Ser682	Ser282
Ser681	Pro287
Thr556	Leu175
Val557	Ile176
Lys551	Lys167
Ala547	Glu161
Asp760	Asp328
Asp623	Asp238
Arg553	Lys172
Ala558	Glu177
Tyr619	Tyr234
Pro620	Thr235
Arg624	Ala239
Asp684	Unknown
Thr680	Met286
Ser759	Gly327
Ala550	Ser164
Glu857	Ser290
Tyr925	Unknown
Asp761	Asp329

Active site residues of SARS-CoV-2-RdRp (PDB ID: 7BTF) and poliovirus-RdRp (PDB ID: 2ILY) are represented.

Note* Comparable residues in the table were results of the superimposition analysis of SARS-CoV-2-RdRp (PDB ID: 7BTF) and poliovirus-RdRp (PDB ID: 2ILY).

chloroquine (Figure 5(d)). Asp623 makes two direct H-bond with the chloroquine while Asp684, Thr687, Ser681, and Asp760 make H-bond through water molecules. Asp684, Thr687, and Ser681 receive H-bond from the chloroquinoline part of the chloroquine and these bonds are formed through the water molecule so-called water bridges. Asp760 also makes H-bond through water molecule, while Asp623 makes two direct H-bond one with the chloroquinoline part and another with the tail part of chloroquine. Ser759 makes one direct H-bond with the tail part of the chloroquine. Asp623 belongs to motif A, while Ser681, Asp684, Asp687 belong to motif B. Ser759 and Asp760 belong to motif C (Figure 5(d)).

Protein–ligand contacts (SARS-CoV-2-RdRp-chloroquine) (Figure 6(d)) show that Asp623, Ser681, Asp684, Thr687, Ser759, and Asp760 show strong interaction during the simulation. It was observed that Asp623, Asp684, Ser759, and Asp760 are showing strong H-bond interaction, while Ser681 and Thr687 are showing good H-bond interaction through the water molecule. Asp623 shows H-bond as well as ionic interaction while Asp684 and Asp760 show H-bond, ionic, and water bridge interactions.

Upon analysis of total contacts (SARS-CoV-2-RdRp-chloroquine) over the full simulation time, it was observed that the maximum number of bonds or contacts formed from 2 to 5 ns and after 23–32 ns (Supporting information Figure 4(a)). The timeline representation of the interactions and contacts

represents that Asp623, Asp684, Asp760, Ser681, and Ser759 exhibit the interactions with the chloroquine. Asp623, Asp684, Asp759, and Asp760 reflect strong interactions throughout the 100 ns of simulation, while Ser681 and Thr687 show the interaction around 44 ns of the simulation, but these interactions are weak as compared to the previously defined residues (Supporting information Figure 4(b)).

RMSD analysis of the SARS-CoV-2-RdRp-chloroquine complex showed that fluctuation in the protein-RMSD became stable around 10 ns and a fluctuation in the protein-RMSD was observed between 75 and 82 ns after that this became stable again. In the case of ligand-RMSD, it also became stable after 10 ns and remained stable till the end of the 100 ns simulation. The RMSD mean for backbone, side-chain, and ligand are 2.961 ± 0.543 , 3.813 ± 0.498 , and 1.678 ± 0.263 Å, respectively (Figure 7(d)).

Besides this, for all the four compounds including ATP, the SEA, SQA, and protein–ligand interaction during the simulation also support the same. Also, the total and potential energy (kcal/mol) of the molecules was good with a minor standard deviation. Importantly, the protein–ligand interaction throughout the simulation also strongly supported the stability of the complex. The ligand seems to be interacting with the same cavity of protein during the entire duration of the simulation in all four compounds.

4. Discussion

RNA-dependent RNA polymerases of various viruses have almost the same structure and morphology and share the same building blocks, i.e. palm, thumb, and finger domains (Kirchdoerfer & Ward, 2019). These domains have seven motifs A-G, in the case of SARS-CoV-2-RdRp, all seven motifs are in the palm domain, these domains and motifs make a grip that serves as a nucleotide and template binding site (Gao et al., 2020). The fingers and the thumb domains remain highly conserved and the RNA/NTP binding grip is also highly conserved. The binding site/active site chamber is connected to the outside by three positively charged tunnels; template entry, nucleotide entry, and product exit tunnels (Figure 1(b,c)) (Gao et al., 2020).

Since the druggable binding site of SARS-CoV-2-RdRps is unknown and no crystal structure of SARS-CoV-2-RdRp with its substrate is available, hence crystal structure available for PV-RdRp (PDB ID: 2ILY) was used in this study as a reference structure. The crystal structure of SARS-CoV-2-RdRp without any substrate or inhibitor (PDB ID: 7BTF) was superimposed over PV-RdRp co-crystallized with ATP (PDB ID: 2ILY), and its binding site was determined and analyzed. Since the structure of PV-RdRp is quite small (461 AA) as compared to SARS-CoV-2-RdRp (932 AA), so we focused only on the active/binding site of both the proteins and we found it to be perfectly superimposed (Figure 2(a–c)).

After superimposition, we compared the SARS-CoV-2-RdRp bound substrate and compounds/inhibitors with the ATP bound PV-RdRp, and analyses were performed. While analyzing the ATP binding site in PV-RdRp, its important residues were compared with the binding site of SARS-CoV-2-RdRp

which are mentioned in Table 3. A 2D interaction diagram showing the important residues around the active site of SARS-CoV-2-RdRp and PV-RdRp are represented in Figure 3(a,b).

A self-prepared library of antimalarials and antiviral compounds was screened against the SARS-CoV-2-RdRp, and three well-known antimalarials chloroquine, hydroxychloroquine, and amodiaquine were observed to be possessing the highest affinity towards SARS-CoV-2-RdRp. All the nucleotides were also screened against SARS-CoV-2-RdRp, and the SARS-CoV-2-RdRp-ATP complex was taken as the reference complex for comparing with the other antimalarial compounds in complex with SARS-CoV-2-RdRp. MMGBSA of the most potent compounds were also determined. After docking and screening, the complexes of these potent antimalarials with SARS-CoV-2-RdRp, and SARS-CoV-2-RdRp-ATP have been subjected to 100 ns MD simulation. Complexes of SARS-CoV-2-RdRp with antimalarials and reference compound ATP were analyzed and compared before and after MD simulations for their binding and other parameters.

ATP being one of the substrates of SARS-CoV-2-RdRp shows the strong interaction with SARS-CoV-2-RdRp (Figure 4(a)). It establishes H-bond interactions with Asp623, Thr680, Asp759, Asp760, Ala550, Arg553, and Arg555. These interactions are comparable to the residues Asp238, Met286, Gly327, Asp328, Ser164, Lys172, and Arg174 of the PV-RdRp crystal structure (co-crystallized with ATP) (PDB ID: 2ILY) (Figure 2(c)).

The co-crystallized structure of PV-RdRp with ATP indicates that these residues are involved in making interactions with ATP (Thompson et al., 2007). After MD simulation, the SARS-CoV-2-RdRp-ATP complex shows main interactions with the Asp623, Lys621, Arg624, Arg553, Arg555, and Lys551 which are comparable to Asp238, Gly236, Ala239, Lys172, Arg174, and Lys167, respectively, of PV-RdRp (Figures 5(a) and 2(c)). It demonstrates that after simulation or during simulation, ATP remains stable in the same pocket. The residues, Asp623, Lys621, Arg555, and Arg553 are commonly interacting residues after and during the simulation. This result suggests that during the simulation, ATP remains stable in the pocket/binding site, and the bonds which are common before and after simulation are very strong and stable.

Docking studies of chloroquine with SARS-CoV-2-RdRp showed that chloroquine had strong interactions with the Thr680, Asp623, and Asn691 whereas the surrounding residues were Arg553, Arg555, Thr556, and Ser681 which were comparable to Met286, Lys172, Asn297, Lys172, Arg174, Leu175, and Pro287 of PV-RdRp, respectively (Figures 4(d) and 2(c)). During and after 100 ns of MD simulation chloroquine showed strong interactions with the Asp623, Asp684, Thr687, Asp760, Ser681, and Ser759, which were comparable to the Lys172, Asp684, Thr293, Asp328, Pro287, and Gly327 of PV-RdRp (Figures 5(d) and 2(c)). Chloroquine also shows H-bond interaction with the Thr680 directly and with Asn691 through water molecule (Figure 6(d)).

Docking results of amodiaquine with SARS-CoV-2-RdRp depict that amodiaquine strongly interacts with the residues

Asp623, Thr680, and Asp760. While the surrounding residues were the same as in the case of chloroquine, the interacting residues were comparable to Asp238, Met286, and Asp328 of PV-RdRp (Figures 4(b) and 2(c)). During MD simulation amodiaquine showed strong interactions with the Asp623, Thr680, Asp760, and Ser759 and these residues were comparable to Asp238, Met286, Asp328, and Gly327 of PV-RdRp (Figure 5(b) and 2(c)).

Similarly, the docking results of hydroxychloroquine with SARS-CoV-2-RdRp suggest that hydroxychloroquine strongly interacts with the Asp623 and Thr680. It is surrounded by Val557, Lys621, Cys622, Asp760, Ser 682, Asn691, which are comparable to the PV-RdRp's Asp238, Met286, Ile176, Gly236, Tyr237, Asp328, Ser282, and Asn297 (Figure 4(c) and 2(c)). During MD simulation, the residues Asp623, Thr680, Asp760, and Asp761 interact strongly with SARS-CoV-2-RdRp which is comparable to Asp238, Met286, Asp328, and Asp329 residues of PV-RdRp (Figure 5(c) and 2(c)).

This comparative analysis suggests that our selected screened and docked compounds are binding at the appropriate binding/active site, and the substrates and inhibitors are not leaving the binding/active site during the simulation. It is reflected as a good sign of the strong and stable binding of a compound at the binding/active site.

Binding site analysis delineated the important residues involved in the interaction. The residues Asp623, Thr680, Asp759, Asp760, Ala550, Arg553, Thr556, Arg555, and Ser681 were the important residues, which participated in the binding of the substrate or inhibitory antimalarial compounds and constructed the appropriate environment for the activity or inhibition. Out of these, Asp623, Thr680, and Asp760 were the most important residues which made strong H-bond interaction with the compounds and substrates. The residue, Asp760, present in motif C (753-FSMMILSDDAVVCFN-767) was involved in the catalytic activity, which was already proven by the mutational study of PV-RdRp (Jablonski & Morrow, 1995). In the present study, we found that the compounds, chloroquine, hydroxychloroquine, amodiaquine, and ATP were making strong H-bond interactions with Asp760, which suggests that these molecules were binding at the active site and the correct position.

The docking results and docked poses of chloroquine, hydroxychloroquine, amodiaquine, and ATP showed a higher affinity towards the SARS-CoV-2-RdRp (Table 1 and Figure 4). The docking scores and further MMGBSA study proved it. Docking scores of the ATP, amodiaquine, hydroxychloroquine, and chloroquine were calculated to be -4.751 , -3.759 , -4.322 , and -4.008 respectively (Table 1). In this study we observed that docking scores of the reference compound and the inhibitory compounds were almost similar, this suggests that inhibitory compounds exhibited the same level of affinity and interactions towards SARS-CoV-2-RdRp. Further MMGBSA study was performed and binding energies were calculated for each compound and these were found to be -26.392 , -39.069 , -46.873 , and -42.653 for ATP, amodiaquine, hydroxychloroquine, and chloroquine, respectively (Table 1). MMGBSA study results showed that inhibitory compounds exhibit higher affinity with the SARS-CoV-2-RdRp

as compared to the reference compound or substrate ATP. Both the docking and MMGBSA studies thus, suggested that inhibitory compounds reflected higher binding affinity as compared to the reference compound ATP. Further, the MD simulation studies for the reference and inhibitory compounds showed energetically favorable residues, which provided a clearer insight into the binding mode with structurally conserved RdRp motifs in the palm subdomain.

The RMSD values for backbone, side-chain, and ligands were calculated for all the inhibitory and reference compounds. The reference compound ATP showed very promising RMSD results. For the SARS-CoV-2-RdRp-ATP complex, values of RMSD mean for backbone, side-chain, and ligand were 2.827 ± 0.216 , 3.696 ± 0.231 , and 2.123 ± 0.195 Å, respectively. The real-time RMSD plot also illustrated that C- α of protein was stable throughout the simulation of 100 ns with a maximum deviation of 3.691 Å with an average value of 2.805 ± 0.217 Å. The deviation in the RMSD value for ligand during the simulation was recorded maximum up to 2.526 Å.

Similarly, antimalarial compounds amodiaquine, hydroxychloroquine, and chloroquine in complex with SARS-CoV-2-RdRp also showed promising RMSD values. RMSD mean values of SARS-CoV-2-RdRp-*amodiaquine* for backbone, side-chain, and ligand were calculated to be 2.947 ± 0.276 , 3.807 ± 0.306 , and 0.935 ± 0.271 Å, respectively. In the case of SARS-CoV-2-RdRp-*amodiaquine* C- α of protein was stable throughout the 100 ns of simulation with a maximum deviation of 3.529 Å with an average value of 2.915 ± 0.275 and the deviation in the RMSD value for ligand during the simulation was found maximum up to 4.404 Å. For SARS-CoV-2-RdRp-*hydroxychloroquine* RMSD mean values for backbone, side-chain, and ligand were calculated to be 2.947 ± 0.261 , 3.770 ± 0.297 , and 2.006 ± 0.278 Å, respectively. In the case of SARS-CoV-2-RdRp-*hydroxychloroquine* C- α of protein was stable throughout the simulation of 100 ns with a maximum deviation of 3.492 Å with an average value of 2.914 ± 0.262 and the deviation in the RMSD value for ligand during the simulation was recorded maximum up to 2.728 Å. And in the case of SARS-CoV-2-RdRp-*chloroquine* RMSD mean values for backbone, side-chain, and ligand were recorded to be 2.961 ± 0.543 , 3.813 ± 0.498 , and 1.678 ± 0.263 Å, respectively. And in this case, C- α of protein was found stable throughout the simulation of 100 ns with a maximum deviation of 4.656 Å with an average value of 2.928 ± 0.545 , and the deviation in the RMSD value for ligand during the simulation was recorded maximum up to 2.302 Å.

RMSD results of reference and inhibitory compounds showed that the protein alone (apoprotein) and protein with the compounds (conjugate protein) remained stable and the binding of the compounds with the protein was strong and stable during the simulation. In all these cases, RMSD values for backbone were found below 3 Å, which suggested the strong binding and stability of the ligand within the active site of the protein during the simulation.

The protein–ligand contact results suggested that during MD simulation residues Asp623 and Asp760 were common in the reference as well as other inhibitory antimalarial compounds, these residues made strong H-bond interactions.

(Figures 5 and 6) These interactions were observed during the almost full time of the MD simulation (Supporting information Figures 1–4). Thr680 was also found common in the inhibitory compounds but it was less promising in the case of ATP. In the initial dock poses, Asp623 and Thr680 were found common in all the compounds including ATP. This analysis thus suggested that during the simulation and before simulation all the compounds remained in the same binding/active site and exhibited the almost same binding pattern of compounds. The binding pattern of the inhibitory compounds was found very much similar to the reference compound ATP. As we already compared with reference to the PV-RdRp, the data clearly suggested that ATP in SARS-CoV-2-RdRp was binding in the same cavity.

Since our study is on SARS-CoV-2-RdRp therefore we focused on the RdRps inhibitors. Most of the RdRps inhibitors are nucleoside analogues. Nucleoside analogues of adenine and guanine derivatives inhibit the RNA-dependent RNA polymerase and block the viral RNA synthesis (De Clercq, 2019).

Favipiravir is an analogue of guanine and it is effective against RdRps of many RNA viruses like ebola, chikungunya, influenza, yellow fever, norovirus, enterovirus, etc. (De Clercq, 2019). A recent study showed the effect of favipiravir against SARS-CoV-2 in Vero cell line (Wang et al., 2020). Since March 2020 to June 2020 Italy, Russia, and India have approved the use of favipiravir for the treatment of COVID-19. Ribavirin is also a guanine derivative which is a known drug for the treatment of the Hepatitis C and respiratory and syncytial virus (RSV), it is also tested for the treatment of SARS and MERS but this showed some severe side effects like anemia at high doses (Zumla et al., 2016). A randomized trial of ribavirin with pegylated interferon against COVID-19 has been performed (ChiCTR2000029387). Although this is still not clear that pegylated interferon with a nucleoside compound will work synergistically against SARS-CoV-2. Galidesivir-BCX4430 is an adenosine analogue that was originally developed for the treatment of hepatitis C, further, this drug was developed for the treatment of Ebola virus disease, Marburg virus disease, and Zika virus (Warren et al., 2014). Galidesivir-BCX4430 is also found effective for the treatment of COVID-19, and presently galidesivir-BCX4430 is under phase 2 human trial in Brazil and various locations around the world for COVID-19 (Warren et al., 2014).

Remdesivir is the most potent drug of the RdRps inhibitor class (Gordon et al., 2020; Li & De Clercq, 2020). It is an adenosine nucleotide analogue prodrug and the most promising antiviral against coronaviruses. On May 1, 2020 US FDA approved the emergency use of remdesivir for hospitalized COVID-19 patients. Further use of remdesivir was approved for moderate COVID-19 disease also on August 28, 2020. Remdesivir inhibits the replication of coronaviruses in the epithelial cells of the respiratory tract. In recent studies, it was observed that remdesivir competes with the substrate ATP during RNA replication and added itself to the growing chain, and causes the termination of chain elongation (Gordon et al., 2020).

A recently cryo-EM study revealed the binding of the remdesivir with the SARS-CoV-2-RdRp (PDB ID: 7BV2) (Figure 8) (Yin et al., 2020). Figure 8 generated by using PDB ID: 7BV2 shows the remdesivir bounded SARS-CoV-2-RdRp, here the main interacting residues of SARS-CoV-2-RdRp which are binding to remdesivir are Lys545, Arg555, Asp623, and Asp760 and the residues which are in the surrounding of the

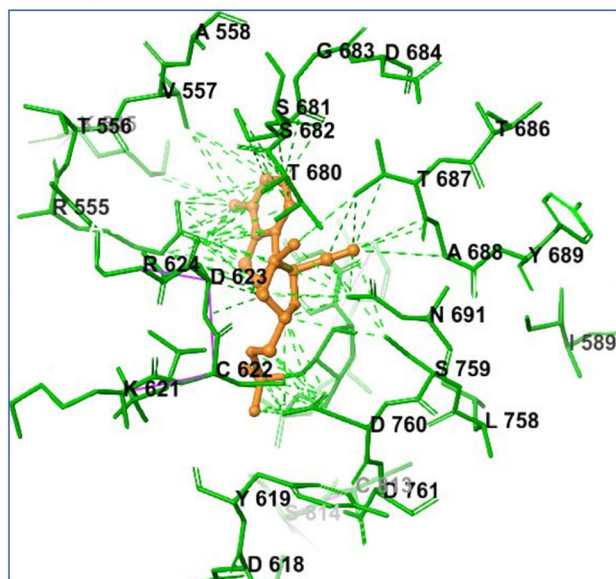


Figure 8. SARS-CoV-2-Remdesivir complex, showing the main interactions with the residues. Figure was generated using the PDB ID: 7BV2.

remdesivir binding site are Asp623, Asp761, Thr680, Asn691, Cys622, Ser681, and Ser682. We compared our docking and simulation results showing the interactions of antimalarials (amodiaquine, hydroxychloroquine, and chloroquine) with the SARS-CoV-2-RdRp (Figures 4 and 5) with the remdesivir-bounded SARS-CoV-2-RdRp (Figure 8). In our study, the main residues of the SARS-CoV-2-RdRp which are binding with are antimalarial compound (amodiaquine, hydroxychloroquine, and chloroquine) are Asp623, Thr680, and Asp 760. On comparison of the surrounding residues of the remdesivir bounded SARS-CoV-2-RdRp and antimalarials-bounded SARS-CoV-2-RdRp, it was observed that almost all the surrounding residues are similar in both cases. This also suggests that in our case binding of antimalarials amodiaquine, hydroxychloroquine, and chloroquine are at the correct place in the SARS-CoV-2-RdRp. Besides this, the Asp760 is the main catalytic residue of the RdRps activity and it was observed that all the antimalarial took by us showing the binding with the Asp760 (Figure 4).

Since the coronaviruses have exonuclease proofreading activity and this activity is performed by the nsp14 (Bouvet et al., 2012; Ma et al., 2015; Minskaia et al., 2006; Snijder et al., 2003). Therefore, the nucleoside analogue based drugs may not be successful or less successful. In our case antimalarials are non-nucleoside-based drugs and these drugs may not be affected by the exonuclease activity of SARS-CoV-2. Therefore, treatment with non-nucleoside-based drugs has an advantage in the case of SARS-CoV-2 treatment.

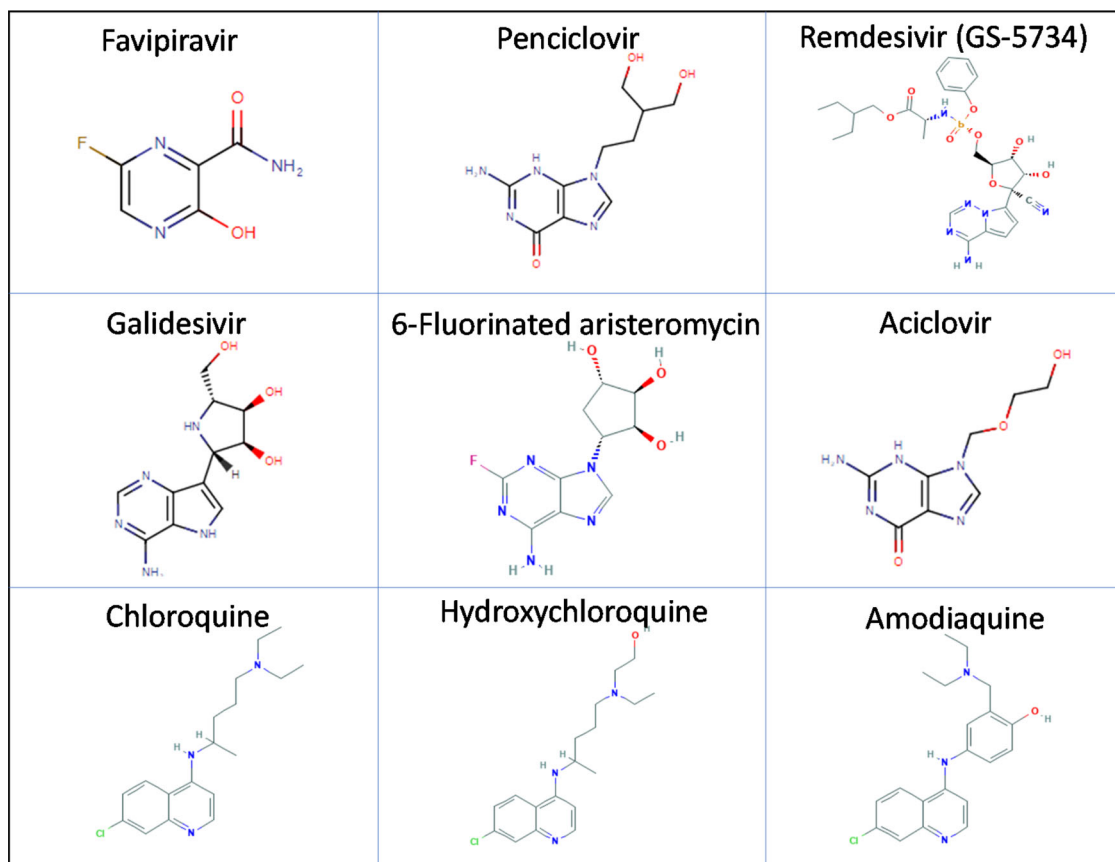


Figure 9. Structural comparison of SARS-CoV-2-RdRp specific antivirals and antimalarials used in this study. Structures of SARS-CoV-2-RdRp specific antivirals shown in the upper two panels and amodiaquine, chloroquine, and hydroxychloroquine are in the lower panel.

Nucleosides consist of a purine or a pyrimidine base, and purines and pyrimidines are N-heterocyclic compounds. Purines consist of a pyrimidine (six-membered) ring and one imidazole (five-membered) ring, both rings contain two N-atom concerning 1, 3 positions. Most of the antiviral drugs like favipiravir, penciclovir, remdesivir-5734, galidesivir, 6'-fluorinated aristeromycin, and acyclovir consist of purine scaffold (Figure 9). However, antimalarials drugs such as amodiaquine, chloroquine, and hydroxychloroquine are non-nucleoside-based drugs. These drugs belong to the quinoline class of compounds. Quinolines are bicyclic compounds consist of a benzene ring fused with a pyridine ring.

General observation suggest that antimalarials are non-nucleoside-based drugs, but mimic of purines scaffolds. The structural similarity may allow the antimalarials to go at the active site of the SARS-CoV-2-RdRp protein. As we discussed that the antimalarials and the remdesivir share the almost same residues and bind in the same pocket. Therefore, overall results suggest that the binding of antimalarials taken in our study are binding at the appropriate place with good affinity. And this should be also free from the exonuclease proofreading activity of nsp14 of SARS-CoV-2.

5. Conclusions

In this multistep computational study, we have shown that the antimalarials such as chloroquine, hydroxychloroquine, and amodiaquine are binding to the active site of SARS-CoV-2-RdRp, in the same manner as its substrate ATP binds. Since any crystal structure of SARS-CoV-2-RdRp bounded with its substrate or inhibitor is not available, therefore we used the crystal structure of PV-RdRp complexed with ATP and compared the interacting residues. The MMGBSA and MD simulations studies suggested that the binding of antimalarials with SARS-CoV-2-RdRp were quite strong and stable and within the active site. Further, we also compared our results with the recently discovered remdesivir bounded SARS-CoV-2-RdRp structure, these results also suggested that antimalarials that we used in our study are binding strongly and within the active site. This is the first report which has generated a lead and evidence to demonstrate that antimalarials may be used as the direct inhibitors of SARS-CoV-2-RdRp. Further *in vitro* and *in vivo* studies are required to support our *in silico* findings.

Acknowledgements

We are also thankful to Ms. Priyanka Tiwari, Department of Biochemistry, University of Allahabad, Allahabad, for her technical support. The authors are grateful to UGC-SAP and DST-FIST for their generous support towards creating research facilities at the Department of Biochemistry of the University of Allahabad, Allahabad, India.

Disclosure statement

The authors declare that they do not have any conflicts of interest.

Funding

PKD is thankful to UGC-New Delhi for supporting him in the form of a Dr. D.S. Kothari Post-Doctoral Research Fellowship. BS acknowledges UPCST-Lucknow for the support in the form of a Research Grant.

ORCID

Pritish Kumar Varadwaj  <http://orcid.org/0000-0001-5706-2411>

References

- Ago, H., Adachi, T., Yoshida, A., Yamamoto, M., Habuka, N., Yatsunami, K., & Miyano, M. (1999). Crystal structure of the RNA-dependent RNA polymerase of hepatitis C virus. *Structure (London, England: 1993)*, 7(11), 1417–1426. [https://doi.org/10.1016/S0969-2126\(00\)80031-3](https://doi.org/10.1016/S0969-2126(00)80031-3)
- Agostini, M. L., Andres, E. L., Sims, A. C., Graham, R. L., Sheahan, T. P., Lu, X., Smith, E. C., Case, J. B., Feng, J. Y., Jordan, R., Ray, A. S., Cihlar, T., Siegel, D., Mackman, R. L., Clarke, M. O., Baric, R. S., & Denison, M. R. (2018). Coronavirus susceptibility to the antiviral remdesivir (GS-5734) is mediated by the viral polymerase and the proofreading exonuclease. *mBio*, 9(2), e00221-18. <https://doi.org/10.1128/mBio.00221-18>
- Ahn, D.-G., Choi, J.-K., Taylor, D. R., & Oh, J.-W. (2012). Biochemical characterization of a recombinant SARS coronavirus nsp12 RNA-dependent RNA polymerase capable of copying viral RNA templates. *Archives of Virology*, 157(11), 2095–2104. <https://doi.org/10.1007/s00705-012-1404-x>
- Al-Tawfiq, J. A., Momattin, H., Dib, J., & Memish, Z. A. (2014). Ribavirin and interferon therapy in patients infected with the Middle East respiratory syndrome coronavirus: An observational study. *International Journal of Infectious Diseases*, 20, 42–46. <https://doi.org/10.1016/j.ijid.2013.12.003>
- Appleby, T. C., Perry, J. K., Murakami, E., Barauskas, O., Feng, J., Cho, A., Fox, D., Wetmore, D. R., McGrath, M. E., Ray, A. S., Sofia, M. J., Swaminathan, S., & Edwards, T. E. (2015). Viral replication. Structural basis for RNA replication by the hepatitis C virus polymerase. *Science (New York, N.Y.)*, 347(6223), 771–775. <https://doi.org/10.1126/science.1259210>
- Arabi, Y. M., Shalhoub, S., Mandourah, Y., Al-Hameed, F., Al-Omari, A., Al Qasim, E., Jose, J., Alraddadi, B., Almotairi, A., Al Khatib, K., Abdulmomen, A., Qushmaq, I., Sindi, A. A., Mady, A., Solaiman, O., Al-Raddadi, R., Maghrabi, K., Ragab, A., Al Mekhlafi, G. A., ... Fowler, R. (2020). Ribavirin and interferon therapy for critically ill patients with Middle East respiratory syndrome: A multicenter observational study. *Clinical Infectious Disease*, 70(9), 1837–1844. <https://doi.org/10.1093/cid/ciz544>
- Bouvet, M., Imbert, I., Subissi, L., Gluais, L., Canard, B., & Decroly, E. (2012). RNA 3'-end mismatch excision by the severe acute respiratory syndrome coronavirus nonstructural protein nsp10/nsp14 exonuclease complex. *Proceedings of the National Academy of Sciences of the United States of America*, 109(24), 9372–9377. <https://doi.org/10.1073/pnas.1201130109>
- Bowers, K. J., Chow, D. E., Xu, H., Dror, R. O., Eastwood, M. P., Gregersen, B. A., Klepeis, J. L., Kolossvary, I., Moraes, M. A., Sacerdoti, F. D., Salmon, J. K., Shan, Y., & Shaw, D. E. (2006). *Scalable algorithms for molecular dynamics simulations on commodity clusters* SC '06: Proceedings of the 2006 ACM/IEEE Conference on Supercomputing, pp. 43–43. <https://doi.org/10.1109/SC.2006.54>
- Brown, A. J., Won, J. J., Graham, R. L., Dinnon, K. H., Sims, A. C., Feng, J. Y., Cihlar, T., Denison, M. R., Baric, R. S., & Sheahan, T. P. (2019). Broad spectrum antiviral remdesivir inhibits human endemic and zoonotic deltacoronaviruses with a highly divergent RNA dependent RNA polymerase. *Antiviral Research*, 169, 104541. <https://doi.org/10.1016/j.antiviral.2019.104541>
- Centers for Disease Control and Prevention (CDC). (2003). Update: Severe acute respiratory syndrome – United States, June 11, 2003. *MMWR. Morbidity and Mortality Weekly Report*, 52(23), 550.

- Chong, C. R., & Sullivan, D. J. (2003). Inhibition of heme crystal growth by antimalarials and other compounds: Implications for drug discovery. *Biochemical Pharmacology*, 66(11), 2201–2212. <https://doi.org/10.1016/j.bcp.2003.08.009>
- Coronavirus Disease (COVID-19) Situation Reports. (n.d.). Retrieved July 10, 2020, from <https://www.who.int/emergencies/diseases/novel-coronavirus-2019/situation-reports>
- De Clercq, E. (2019). New nucleoside analogues for the treatment of hemorrhagic fever virus infections. *Chemistry, an Asian Journal*, 14(22), 3962–3968. <https://doi.org/10.1002/asia.201900841>
- de Wilde, A. H., Jochmans, D., Posthuma, C. C., Zevenhoven-Dobbe, J. C., van Nieuwkoop, S., Bestebroer, T. M., van den Hoogen, B. G., Neyts, J., & Snijder, E. J. (2014). Screening of an FDA-approved compound library identifies four small-molecule inhibitors of Middle East respiratory syndrome coronavirus replication in cell culture. *Antimicrobial Agents and Chemotherapy*, 58(8), 4875–4884. <https://doi.org/10.1128/AAC.03011-14>
- Falzarano, D., de Wit, E., Rasmussen, A. L., Feldmann, F., Okumura, A., Scott, D. P., Brining, D., Bushmaker, T., Martellaro, C., Baseler, L., Benecke, A. G., Katze, M. G., Munster, V. J., & Feldmann, H. (2013). Treatment with interferon- α 2b and ribavirin improves outcome in MERS-CoV-infected rhesus macaques. *Nature Medicine*, 19(10), 1313–1317. <https://doi.org/10.1038/nm.3362>
- Ferrer-Orta, C., Arias, A., Escarmís, C., & Verdaguer, N. (2006). A comparison of viral RNA-dependent RNA polymerases. *Current Opinion in Structural Biology*, 16(1), 27–34. <https://doi.org/10.1016/j.sbi.2005.12.002>
- Fox, R. I. (1993). Mechanism of action of hydroxychloroquine as an anti-rheumatic drug. *Seminars in Arthritis and Rheumatism*, 23(2 Suppl 1), 82–91. [https://doi.org/10.1016/S0049-0172\(10\)80012-5](https://doi.org/10.1016/S0049-0172(10)80012-5)
- Gao, Y., Yan, L., Huang, Y., Liu, F., Zhao, Y., Cao, L., Wang, T., Sun, Q., Ming, Z., Zhang, L., Ge, J., Zheng, L., Zhang, Y., Wang, H., Zhu, Y., Zhu, C., Hu, T., Hua, T., Zhang, B., ... Rao, Z. (2020). Structure of the RNA-dependent RNA polymerase from COVID-19 virus. *Science (New York, N.Y.)*, 368(6492), 779–782. <https://doi.org/10.1126/science.abb7498>
- Gong, P., & Peersen, O. B. (2010). Structural basis for active site closure by the poliovirus RNA-dependent RNA polymerase. *Proceedings of the National Academy of Sciences of the United States of America*, 107(52), 22505–22510. <https://doi.org/10.1073/pnas.1007626107>
- Gorbalenya, A. E., Baker, S. C., Baric, R. S., de Groot, R. J., Drosten, C., Gulyaeva, A. A., Haagmans, B. L., Lauber, C., Leontovich, A. M., Neuman, B. W., Penzar, D., Perlman, S., Poon, L. L. M., Samborskiy, D. V., Sidorov, I. A., Sola, I., & Ziebuhr, J. & Coronaviridae Study Group of the International Committee on Taxonomy of Viruses. (2020). The species severe acute respiratory syndrome-related coronavirus: Classifying 2019-nCoV and naming it SARS-CoV-2. *Nature Microbiology*, 5(4), 536–544. <https://doi.org/10.1038/s41564-020-0695-z>
- Gordon, C. J., Tchesnokov, E. P., Feng, J. Y., Porter, D. P., & Götte, M. (2020). The antiviral compound remdesivir potently inhibits RNA-dependent RNA polymerase from Middle East respiratory syndrome coronavirus. *The Journal of Biological Chemistry*, 295(15), 4773–4779. <https://doi.org/10.1074/jbc.AC120.013056>
- Halgren, T. A., Murphy, R. B., Friesner, R. A., Beard, H. S., Frye, L. L., Pollard, W. T., & Banks, J. L. (2004). Glide: A new approach for rapid, accurate docking and scoring. 2. Enrichment factors in database screening. *Journal of Medicinal Chemistry*, 47(7), 1750–1759. <https://doi.org/10.1021/jm030644s>
- Hansen, J. L., Long, A. M., & Schultz, S. C. (1997). Structure of the RNA-dependent RNA polymerase of poliovirus. *Structure (Structure)*, 5(8), 1109–1122. [https://doi.org/10.1016/S0969-2126\(97\)00261-X](https://doi.org/10.1016/S0969-2126(97)00261-X)
- Hayes, J. M., & Archontis, G. (2012). MM-GB(PB)SA calculations of protein–ligand binding free energies. *Molecular Dynamics – Studies of Synthetic and Biological Macromolecules* (pp. 171–190). In tech. ISBN: 978-953-51-0444-5. <https://doi.org/10.5772/37107>
- Jablonski, S. A., & Morrow, C. D. (1995). Mutation of the aspartic acid residues of the GDD sequence motif of poliovirus RNA-dependent RNA polymerase results in enzymes with altered metal ion requirements for activity. *Journal of Virology*, 69(3), 1532–1539. <https://doi.org/10.1128/JVI.69.3.1532-1539.1995>
- Jorgensen, W. L., Chandrasekhar, J., Madura, J. D., Impey, R. W., & Klein, M. L. (1983). Comparison of simple potential functions for simulating liquid water. *The Journal of Chemical Physics*, 79(2), 926–935. <https://doi.org/10.1063/1.445869>
- Kim, U. J., Won, E.-J., Kee, S.-J., Jung, S.-I., & Jang, H.-C. (2016). Combination therapy with lopinavir/ritonavir, ribavirin and interferon- α for Middle East respiratory syndrome. *Antiviral Therapy*, 21(5), 455–459. <https://doi.org/10.3851/IMP3002>
- Kirchdoerfer, R. N., & Ward, A. B. (2019). Structure of the SARS-CoV nsp12 polymerase bound to nsp7 and nsp8 co-factors. *Nature Communications*, 10(1), 2342. <https://doi.org/10.1038/s41467-019-10280-3>
- Kupferschmidt, K., & Cohen, J. (2020). Will novel virus go pandemic or be contained? *Science (New York, N.Y.)*, 367(6478), 610–611. <https://doi.org/10.1126/science.367.6478.610>
- Lamb, Y. N., & Deeks, E. D. (2018). Sarilumab: A review in moderate to severe rheumatoid arthritis. *Drugs*, 78(9), 929–940. <https://doi.org/10.1007/s40265-018-0929-z>
- Lehman, K. C., Gulyaeva, A., Zevenhoven-Dobbe, J. C., Janssen, G. M. C., Ruben, M., Overkleeft, H. S., van Veelen, P. A., Samborskiy, D. V., Kravchenko, A. A., Leontovich, A. M., Sidorov, I. A., Snijder, E. J., Posthuma, C. C., & Gorbalenya, A. E. (2015). Discovery of an essential nucleotidylating activity associated with a newly delineated conserved domain in the RNA polymerase-containing protein of all nidoviruses. *Nucleic Acids Research*, 43(17), 8416–8434. <https://doi.org/10.1093/nar/gkv838>
- Li, G., & De Clercq, E. (2020). Therapeutic options for the 2019 novel coronavirus (2019-nCoV). *Nature Reviews Drug Discovery*, 19(3), 149–150. <https://doi.org/10.1038/d41573-020-00016-0>
- Liu, Y., Gayle, A. A., Wilder-Smith, A., & Rocklöv, J. (2020). The reproductive number of COVID-19 is higher compared to SARS coronavirus. *Journal of Travel Medicine*, 27(2), taaa021 <https://doi.org/10.1093/jtm/taaa021>
- Ma, Y., Wu, L., Shaw, N., Gao, Y., Wang, J., Sun, Y., Lou, Z., Yan, L., Zhang, R., & Rao, Z. (2015). Structural basis and functional analysis of the SARS coronavirus nsp14-nsp10 complex. *Proceedings of the National Academy of Sciences of the United States of America*, 112(30), 9436–9441. <https://doi.org/10.1073/pnas.1508686112>
- McDonald, S. M. (2013). RNA synthetic mechanisms employed by diverse families of RNA viruses. *Wiley Interdisciplinary Reviews RNA*, 4(4), 351–367. <https://doi.org/10.1002/wrna.1164>
- Minskaia, E., Hertzog, T., Gorbalenya, A. E., Campanacci, V., Cambillau, C., Canard, B., & Ziebuhr, J. (2006). Discovery of an RNA virus 3'→5' exonuclease that is critically involved in coronavirus RNA synthesis. *Proceedings of the National Academy of Sciences of the United States of America*, 103(13), 5108–5113. <https://doi.org/10.1073/pnas.0508200103>
- Mönttinen, H. A. M., Ravantti, J. J., Stuart, D. I., & Poranen, M. M. (2014). Automated structural comparisons clarify the phylogeny of the right-hand-shaped polymerases. *Molecular Biology and Evolution*, 31(10), 2741–2752. <https://doi.org/10.1093/molbev/msu219>
- Ng, K. K.-S., Arnold, J. J., & Cameron, C. E. (2008). Structure–function relationships among RNA-dependent RNA polymerases. *Current Topics in Microbiology and Immunology*, 320, 137–156. https://doi.org/10.1007/978-3-540-75157-1_7
- Ozdogan, H., & Ugurlu, S. (2017). Canakinumab for the treatment of familial Mediterranean fever. *Expert Review of Clinical Immunology*, 13(5), 393–404. <https://doi.org/10.1080/1744666X.2017.1313116>
- Ridker, P. M., Everett, B. M., Thuren, T., MacFadyen, J. G., Chang, W. H., Ballantyne, C., Fonseca, F., Nicolau, J., Koenig, W., Anker, S. D., Kastelein, J. J. P., Cornel, J. H., Pais, P., Pella, D., Genest, J., Cifkova, R., Lorenzatti, A., Forster, T., Kobalava, Z., ... Glynn, R. J. CANTOS Trial Group (2017). Antiinflammatory therapy with canakinumab for atherosclerotic disease. *The New England Journal of Medicine*, 377(12), 1119–1131. <https://doi.org/10.1056/NEJMoa1707914>
- Sastry, G. M., Adzhigirey, M., Day, T., Annabhimoju, R., & Sherman, W. (2013). Protein and ligand preparation: Parameters, protocols, and influence on virtual screening enrichments. *Journal of Computer-Aided Molecular Design*, 27(3), 221–234. <https://doi.org/10.1007/s10822-013-9644-8>

- Shan, Y., Klepeis, J. L., Eastwood, M. P., Dror, R. O., & Shaw, D. E. (2005). Gaussian split Ewald: A fast Ewald mesh method for molecular simulation. *The Journal of Chemical Physics*, 122(5), 54101. <https://doi.org/10.1063/1.1839571>
- Sheahan, T. P., Sims, A. C., Leist, S. R., Schäfer, A., Won, J., Brown, A. J., Montgomery, S. A., Hogg, A., Babusis, D., Clarke, M. O., Spahn, J. E., Bauer, L., Sellers, S., Porter, D., Feng, J. Y., Cihlar, T., Jordan, R., Denison, M. R., & Baric, R. S. (2020). Comparative therapeutic efficacy of remdesivir and combination lopinavir, ritonavir, and interferon beta against MERS-CoV. *Nature Communications*, 11(1), 222. <https://doi.org/10.1038/s41467-019-13940-6>
- Snijder, E. J., Bredenbeek, P. J., Dobbe, J. C., Thiel, V., Ziebuhr, J., Poon, L. L. M., Guan, Y., Rozanov, M., Spaan, W. J. M., & Gorbalenya, A. E. (2003). Unique and conserved features of genome and proteome of SARS-coronavirus, an early split-off from the coronavirus group 2 lineage. *Journal of Molecular Biology*, 331(5), 991–1004. [https://doi.org/10.1016/S0022-2836\(03\)00865-9](https://doi.org/10.1016/S0022-2836(03)00865-9)
- Su, S., Wong, G., Shi, W., Liu, J., Lai, A. C. K., Zhou, J., Liu, W., Bi, Y., & Gao, G. F. (2016). Epidemiology, genetic recombination, and pathogenesis of coronaviruses. *Trends in Microbiology*, 24(6), 490–502. <https://doi.org/10.1016/j.tim.2016.03.003>
- Tang, B., Bragazzi, N. L., Li, Q., Tang, S., Xiao, Y., & Wu, J. (2020). An updated estimation of the risk of transmission of the novel coronavirus (2019-nCoV). *Infectious Disease Modelling*, 5, 248–255. <https://doi.org/10.1016/j.idm.2020.02.001>
- Te Velthuis, A. J. W. (2014). Common and unique features of viral RNA-dependent polymerases. *Cellular and Molecular Life Science*, 71(22), 4403–4420. <https://doi.org/10.1007/s00018-014-1695-z>
- Te Velthuis, A. J. W., Arnold, J. J., Cameron, C. E., van den Worm, S. H. E., & Snijder, E. J. (2010). The RNA polymerase activity of SARS-coronavirus nsp12 is primer dependent. *Nucleic Acids Research*, 38(1), 203–214. <https://doi.org/10.1093/nar/gkp904>
- Thompson, A. A., Albertini, R. A., & Peersen, O. B. (2007). Stabilization of poliovirus polymerase by NTP binding and fingers-thumb interactions. *Journal of Molecular Biology*, 366(5), 1459–1474. <https://doi.org/10.1016/j.jmb.2006.11.070>
- van der Hoek, L. (2007). Human coronaviruses: What do they cause? *Antiviral Therapy*, 12(4 Pt B), 651–658.
- Wang, M., Cao, R., Zhang, L., Yang, X., Liu, J., Xu, M., Shi, Z., Hu, Z., Zhong, W., & Xiao, G. (2020). Remdesivir and chloroquine effectively inhibit the recently emerged novel coronavirus (2019-nCoV) in vitro. *Cell Research*, 30(3), 269–271. <https://doi.org/10.1038/s41422-020-0282-0>
- Warren, T. K., Wells, J., Panchal, R. G., Stuthman, K. S., Garza, N. L., Van Tongeren, S. A., Dong, L., Retterer, C. J., Eaton, B. P., Pegoraro, G., Honnold, S., Bantia, S., Kotian, P., Chen, X., Taubenheim, B. R., Welch, L. S., Minning, D. M., Babu, Y. S., Sheridan, W. P., & Bavari, S. (2014). Protection against filovirus diseases by a novel broad-spectrum nucleoside analogue BCX4430. *Nature*, 508(7496), 402–405. <https://doi.org/10.1038/nature13027>
- Wu, F., Zhao, S., Yu, B., Chen, Y.-M., Wang, W., Song, Z.-G., Hu, Y., Tao, Z.-W., Tian, J.-H., Pei, Y.-Y., Yuan, M.-L., Zhang, Y.-L., Dai, F.-H., Liu, Y., Wang, Q.-M., Zheng, J.-J., Xu, L., Holmes, E. C., & Zhang, Y.-Z. (2020). A new coronavirus associated with human respiratory disease in China. *Nature*, 579(7798), 265–269. <https://doi.org/10.1038/s41586-020-2008-3>
- Yap, T. L., Xu, T., Chen, Y.-L., Malet, H., Egloff, M.-P., Canard, B., Vasudevan, S. G., & Lescar, J. (2007). Crystal structure of the dengue virus RNA-dependent RNA polymerase catalytic domain at 1.85-Ångstrom resolution. *Journal of Virology*, 81(9), 4753–4765. <https://doi.org/10.1128/JVI.02283-06>
- Yin, W., Mao, C., Luan, X., Shen, D.-D., Shen, Q., Su, H., Wang, X., Zhou, F., Zhao, W., Gao, M., Chang, S., Xie, Y.-C., Tian, G., Jiang, H.-W., Tao, S.-C., Shen, J., Jiang, Y., Jiang, H., Xu, Y., ... Xu, H. E. (2020). Structural basis for inhibition of the RNA-dependent RNA polymerase from SARS-CoV-2 by remdesivir. *Science (New York, N.Y.)*, 368(6498), 1499–1504. <https://doi.org/10.1126/science.abc1560>
- Zhai, Y., Sun, F., Li, X., Pang, H., Xu, X., Bartlam, M., & Rao, Z. (2005). Insights into SARS-CoV transcription and replication from the structure of the nsp7-nsp8 hexadecamer. *Nature Structural & Molecular Biology*, 12(11), 980–986. <https://doi.org/10.1038/nsmb999>
- Zumla, A., Chan, J. F. W., Azhar, E. I., Hui, D. S. C., & Yuen, K.-Y. (2016). Coronaviruses – drug discovery and therapeutic options. *Nature Reviews. Drug Discovery*, 15(5), 327–347. <https://doi.org/10.1038/nrd.2015.37>